THE JOURNAL OF PHYSICAL CHEMISTRY A

ARTICLE

pubs.acs.org/JPCA

Isotope Effects and the Temperature Dependences of the Hyperfine Coupling Constants of Muoniated *sec*-Butyl Radicals in Condensed Phases

Donald G. Fleming,* Michael D. Bridges,† and Donald J. Arseneau

TRIUMF and Department of Chemistry, University of British Columbia, Vancouver, BC v6T 1Z1, Canada

Ya Kun Chen and Yan Alexander Wang

Department of Chemistry, University of British Columbia, vancouver, BC v6T 1Z1, Canada

ABSTRACT: Reported here is the first μSR study of the muon (A_μ) and proton (A_p) β-hyperfine coupling constants (Hfcc) of muoniated *sec*-butyl radicals, formed by muonium (Mu) addition to 1-butene and to *cis*- and *trans*-2-butene. The data are compared with in vacuo spin-unrestricted MP2 and hybrid DFT/B3YLP calculations reported in the previous paper (I), which played an important part in the interpretation of the data. The *T*-dependences of both the (reduced) muon, $A_\mu'(T)$, and proton, $A_p(T)$, Hfcc are surprisingly well explained by a simple model, in which the calculated Hfcc from paper I at energy minima of 0 and near $\pm$120° are thermally averaged, assuming an energy dependence given by a basic 2-fold torsional potential. Fitted torsional barriers to $A_\mu'(T)$ from this model are similar (~3 kJ/mol) for all muoniated butyl radicals, suggesting that these are dominated by ZPE effects arising from the C−Mu bond, but for $A_p(T)$ exhibit wide variations depending on environment. For the *cis*- and *trans*-2-butyl radicals formed from 2-butene, $A_\mu'(T)$ exhibits clear discontinuities at bulk butene melting points, evidence for molecular interactions enhancing these muon Hfcc in the environment of the solid state, similar to that found in earlier reports for muoniated *tert*-butyl. In contrast, for Mu−*sec*-butyl formed from 1-butene, there is no such discontinuity. The muon hfcc for the *trans*-2-butyl radical are seemingly very well predicted by B3LYP calculations in the solid phase, but for *sec*-butyl from 1-butene, showing the absence of further interactions, much better agreement is found with the MP2 calculations across the whole temperature range. Examples of large proton Hfcc near 0 K are also reported, due to eclipsed C−H bonds, in like manner to C−Mu, which then also exhibit clear discontinuities in $A_p(T)$ at bulk melting points. The data suggest that the good agreement found between theory and experiment from the B3LYP calculations for eclipsed bonds in the solid phase may be fortuitous. For the staggered protons of the *sec*-butyl radicals formed, no discontinuities are seen at all in $A_p(T)$, also demonstrating no further effects of molecular interactions on these particular proton Hfcc.

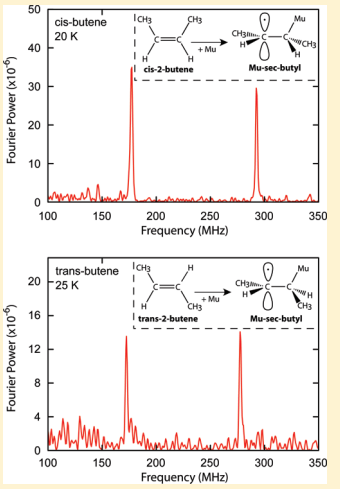

1. INTRODUCTION

The study of the isotropic β-proton hyperfine coupling constants (Hfcc) of simple alkyl radicals by EPR dates back four decades[1−4] (see also ref 5), and includes the first studies of deuterium isotope effects in the classic work of Fessenden and Schuler on the isotopomers of the ethyl radical.[1] Isotopic substitution at the β-position renders the proton environments of the unsubstituted radical inequivalent and gives rise to clear *T*-dependent Hfcc that depend on changing conformations of the radical with temperature, dictated in large part by torsional barriers to internal rotation.

A hydrogen isotope of increasing importance as a spin probe of both hyperfine couplings and molecular conformations of free radicals is the muonium (Mu = μ^+e^-) atom, dating from the first studies of "muoniated" free radicals in liquids in 1978.[6] The μ^+ is produced 100% spin polarized at a nuclear accelerator (TRIUMF in the present study) and this polarization can be effectively transfered to a free radical by Mu addition reactions, and then sensitively monitored by the μSR (muon spin relaxation or resonance) technique.[6−14]

The most extensive studies of Hfcc in alkyl radicals to date has been for the ethyl radical and its isotopomers, both by EPR[1,5,12,15] and μSR[12,14] (see also citations in ref 11). Of relevance here are the torsional barriers to internal rotation. For unsubstituted ethyl, this is thought to be too small to measure experimentally,[1,12,15] though calculated barriers are around 200 J/mol.[16,17] For the β-Hfcc of deuterated ethyl, the barrier was found to be ~350 J/mol,[1,12] consistent with ab initio calculations,[16] with opposite *T*-dependences observed for proton and deuterium Hfcc.[12]

Since the electronic Hamiltonian is isotopically invariant within the Born−Oppenheimer (BO) approximation, the effect of isotopic substitution on torsional barriers is due to differences in zero-point-energy (ZPE) at potential extrema.[12,14,16−20] Given that the muon mass is only one-ninth that of the proton, much larger changes in

Received: June 1, 2010
Revised: December 7, 2010
Published: March 11, 2011

   dx.doi.org/10.1021/jp109676b | *J. Phys. Chem. A* 2011, 115, 2778–2793

torsional barriers can be expected for muoniated alkyl radicals, in comparison with their deuterated counterparts, with barrier heights of ~2−3 kJ/mol for Mu−ethyl,[12,16] Mu−propyl,[18] and Mu−*tert*-butyl[7] radicals. Somewhat paradoxically, for the unsubstituted *tert*-butyl radical, barriers up to ~5 kJ/mol have been reported.[1,3,21] The aforementioned μSR studies have also established that the light muon mass of the C−Mu bond adopts an "eclipsed" conformation near 0° with respect to the p_Z orbital of the unpaired electron at 0 K, with its barrier to internal rotation then manifest by a measurement of the *T*-dependence of the muon Hfcc.

The present paper reports on μSR measurements of both proton and muon Hfcc for the muoniated *sec*-butyl radicals formed from Mu addition to the parent butenes, 1-butene and *cis*- and *trans*-2-butene, over wide temperature ranges in both the solid and liquid phases. Comparisons with earlier data for the muon Hfcc reported for the Mu−*tert*-butyl radical in the solid[7] and liquid[7,22] phases are also made. As with all muoniated radicals formed from Mu addition to alkenes, the muon is placed in a C−Mu bond at the β-carbon, one carbon removed from the radical center.

There are two broad motivations for this study. First, these *sec*-butyl radicals represent good test cases for comparisons with calculational methods of β-Hfcc for more complex alkyl radicals beyond those for the simplest ethyl radical,[23−25] and as well for the *tert*-butyl radical,[7,21,26] as reported in the preceding theory paper, hereafter referred to as "paper I"(Chen, Y. K.; et al. *J. Phys. Chem. A* **2011**, 10.1021/jp1096212). These calculations have employed both spin unrestricted density functional theory (DFT), using the B3LYP density functional, and MP2 calculations with EPR-III basis sets, and will be seen to play an important role in the interpretation of the present data. Second, these same radicals are being studied as part of a parallel investigation of muoniated radicals in zeolites, complementing recent work of the Mu−ethyl radical in the same frameworks,[11] and it is important to have both "benchmark" experiments and calculations in neat environments with which to compare.

2. EXPERIMENTAL SECTION

2.1. Sample Preparation and Environment. The 1-butene and *cis*- and *trans*-2-butene samples were obtained as high vapor pressure liquids from Aldrich Chemicals. A plumbing manifold was connected to the gas sample bottle and to a stainless steel target cell, fitted with a welded thin window (~25 or 50 μm thick), via a Cu tube through which vapor was loaded into the cell. (See ref 11 for more detail.) Target cells were initially kept at a low temperature in a lN_2 bath, well below the melting point of the neat solid. When the target cell was opened to the plumbing, the vapor condensed inside, until there was no further loss of pressure. Several freeze−pump−thaw cycles were carried out to remove any dissolved O_2, which is known to cause extra line broadening in a μSR experiment due to electron (Heisenberg) spin exchange.[27,28] The sample cells were then sealed with a crimping tool and kept in a deep-freeze environment (at −20 C) prior to use.

A given sample cell was mounted in a helium-flow cryostat for temperature control and placed in a superconducting magnet ("Helios") that provided magnetic fields up to 30 kG in these studies, aligned with the beam direction. Experiments were run on the M20 beamline at the TRIUMF cyclotron, which provides a spin-rotated muon beam, so that both longitudinal field (LF) and transverse field (TF) experiments could be carried out within the same setup on the same sample. Spin-polarized surface muons passed through the thin target entrance window and stopped within the sample, forming the muoniated radical of interest. Decay positrons were detected by counter arrays arranged around the beam direction, with events routed to four separate histograms in the case of TF studies and to two histograms for LF (ALC) studies.

All samples were studied as either neat solids or liquids over the temperature range from near 5 to 250 K. Temperature readings were monitored by two different thermocouples attached to the target cell, which typically gave consistent readings to better than 1 deg. It was assumed that this was also the temperature in the sample environment. Systematic errors in cell temperatures over different runs that spanned a 2 year period could be ±2 K though.

2.2. Basics of the μSR Technique. The positive muon (μ^+) is produced 100% spin polarized, and in its decay process ($\mu^+ \rightarrow e^+\nu_e\bar{\nu}_\mu$) the positron is emitted *preferentially* along the muon spin direction, providing a convenient method for detecting the muon polarization.[8,13] In a TF experiment, the muon "asymmetry" at the time of decay, in a time-differential (TD) measurement, is given by

$$A(t) = \sum_i A_i e^{-\lambda_i t} \cos(\omega_i t + \phi_i) \quad (1)$$

where A_i, λ_i, ω_i, and ϕ_i are the initial amplitude, relaxation rate, precession frequency, and initial phase for the *i*th environment. For the Mu radicals of interest, in TFs ≳ 1.5 kG, there are three principal frequencies, corresponding to muons in diamagnetic environments (ν_D) and two radical frequencies, ν_{12} and ν_{34} for a given radical, that correspond to the allowed transitions of the spin Hamiltonian.[8,29] These are most easily seen in Fourier transform (FT-μSR) spectra at the characteristic precession frequencies,[7,8,11,13]

$$\nu_{12} = \left|\frac{1}{2}A_\mu - \nu_m\right| \quad \text{and} \quad \nu_{34} = \nu_m + \frac{1}{2}A_\mu \quad (2)$$

where A_μ is the *isotropic* muon-electron Hfcc and

$$\nu_m = \frac{1}{2}([A_\mu{}^2 + (\nu_e + \nu_D)^2]^{1/2} - \nu_e + \nu_D) \quad (3)$$

with the Zeeman (Larmor) frequencies $\nu_D = \omega_\mu/2\pi = \gamma_\mu B$ for diamagnetic muons (γ_μ = 0.013 55 MHz G^{-1}) and $\nu_e = \gamma_e B$ for the electron (γ_e = 2.8025 MHz G^{-1}), in an applied field, *B*.

Fits to TD decay asymmetries or FT-μSR spectra by eq 1 or 2, while directly giving the muon Hfcc, are not always feasible either due to substantial line-broadening effects, particularly in polycrystalline environments,[30,31] or slow radical formation, which results in dephasing of the muon spin in high transverse fields. In these cases, the muon Hfcc can be found by the ALC-μSR technique in a longitudinal field, which also provides the important measurement of the *nuclear* (here proton only) Hfcc, A_p.[7,8,10,11] An ALC signal appears as a "dip" in the time-integrated decay asymmetry at a particular value of the LF, corresponding to a resonant transfer of muon spin polarization from the backward to the forward direction as the magnetic field is varied.[8,11,13,14,20,31,32] In the present study, typically several sweeps of the LF range were carried out, in alternating directions, incremented in steps of about 100 G, depending on conditions.

There are two principal ALC resonances that are of interest and which reflect different aspects of the spin Hamiltonian.[8,10,31,33] A Δ_0 resonance represents a "flip-flop" exchange of spin polarization between the muon and proton spin, from which the proton Hfcc, A_p is determined. A Δ_1 resonance is a pure muon "spin-flip" and is directly induced only through the coupling of Zeeman states from the *anisotropic* part of the muon-electron hyperfine interaction. It is then always dependent on the angles between the muon spin and the field direction. As previewed above, A_μ can also be found from a TF

experiment, where, as in ALC-μSR, a muon spin-flip arises from transitions induced by the $\mathbf{I}_+^{\mu}$ operator, a correspondence that provides a valuable identification of a Δ_1 line in ALC spectra.

Though hyperfine anisotropy and molecular reorientation of muoniated free radicals can give rise to asymmetric line shapes,[11,30,31,33] in the present study of neat butenes these are invariably symmetric lines and hence are amenable to Lorentzian fits. It is the *positions* of the ALC resonances, $B_r(\Delta_1)$ and $B_r(\Delta_0)$, that are important here and that are well determined from the fits, even for broad line resonances, giving the isotropic Hfcc of interest: for the muon, A_μ, from the Δ_1 resonance, and for the proton, A_p, for each group of magnetic equivalent nuclei, from the Δ_0 resonances, as defined by eqs 4 and 5,

$$B_r(\Delta_1) = \frac{1}{2}\left|\frac{A_\mu}{\gamma_\mu} - \frac{A_\mu}{\gamma_e}\right| \quad (4)$$

$$B_r(\Delta_0) = \frac{1}{2}\left|\frac{A_\mu - A_p}{\gamma_\mu - \gamma_p} - \frac{A_\mu + A_p}{\gamma_e}\right| \quad (5)$$

respectively.[8,10,11] It can be noted from eq 5 that, in contrast to conventional EPR,[5] the ALC-μSR technique is sensitive to the sign as well as the magnitude of the nuclear Hfcc. Since the gyromagnetic ratio $\gamma_p = \gamma_\mu/3.184$, it is convenient to give the muon Hfcc in reduced units, as A'_μ, defined by $A'_\mu = A_\mu/3.184$, providing then a more realistic comparison of muon and proton Hfcc.

3. EXPERIMENTAL RESULTS AND TRENDS: $A'_\mu(T)$ AND $A_P(T)$

As outlined above, the muon Hfcc have been determined from a combination of fitting TD results (eq 1), from FT-μSR spectra (eq 2) and from ALC-μSR spectra, the latter from the positions of the Δ_1 resonances and eq 4. The proton Hfcc are found from the positions of the Δ_0 resonances and eq 5. In some cases of fast TF relaxation rates ($\gtrsim$20 μs^{-1}), where TD fits to the four separate histograms can give inconsistent results, radical frequencies could be more reliably determined directly from FT-μSR spectra. For the ALC-μSR spectra, the data were fit to a background polynomial plus Lorentzian line shapes for the Δ_1 and Δ_0 resonances, as described in refs 11 and 31. The muon and proton Hfcc reported here are invariably averaged values, both from small changes arising from variations in the fits and from different beam periods, which introduces some systematic error as well. Quoted errors in the following tables and figures are combined errors, and range overall from a realistic minimum of 0.5 MHz to a maximum of ~5 MHz, the latter mainly from overly broad/weak ALC lines. Values for both A_μ and A'_μ are given, the minimum error for the latter being assessed as ±0.3 MHz.

3.1. Mu−*sec*-Butyl (and *n*-Butyl) Radicals from 1-Butene. Two different muoniated radical isomers can be formed from Mu addition to 1-butene: the dominant *sec*-butyl radical, $CH_3CH_2\dot{C}HCH_2Mu$, and the primary *n*-butyl radical, $CH_3CH_2CHMuCH_2$, which is much more weakly formed and is only tentatively identified here. As discussed in paper I, of several possible geometric conformers of the 1-butene parent, the most stable is expected to be the "gauche" (or "skew" form[34]). Several possible *n*-butyl or *sec*-butyl conformers could also be formed though, which impacts on the interpretation of the data, as discussed below.

Figure 1 presents FT-μSR spectra at 80 K (top), in the solid phase, and at 92 K (bottom), just above the melting point of 1-butene (88 K), both in a field of 3.45 kG. The inset shows the molecular structure of the *sec*-butyl radical formed. At 80 K only two very broad transitions are seen at frequencies ν_{12}= 148 MHz and ν_{34}= 252 MHz for the *sec*-butyl radical, giving the muon Hfcc $A_\mu(s\text{-Bu})$= 400 ± 3 MHz from eq 2. Both the fast relaxations in the TD spectra and the broad FT lines seen meant that the muon Hfcc for the *sec*-butyl radical at low temperatures were often more reliably determined from the positions of the Δ_1 ALC resonances (and eq 4), though these too are broad. As is typically the case, these FT lines are much sharper in the liquid phase, where the same pair of radical frequencies are seen strongly at 146 and 247 MHz in the bottom spectrum at 92 K, in agreement with the TD fits from eq 1, giving $A_\mu(s\text{-Bu})$= 393 ± 1 MHz, as recorded in Table 1. The other muon entries at higher temperatures in this table were mainly determined from the TF data.

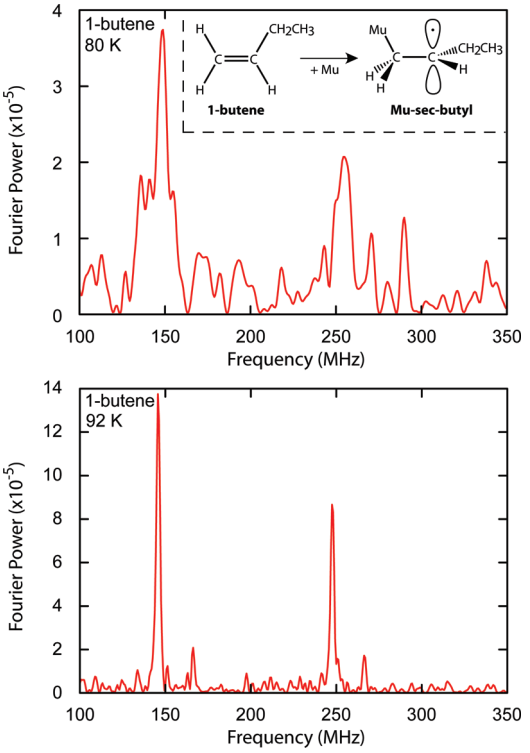

Figure 1. FT-μSR spectra for Mu addition to 1-butene, at 80 K (top) in the solid phase and at 92 K (bottom) in the liquid phase, in a field of 3.45 kG. The inset shows the structure for the dominant *sec*-butyl radical expected to form. In the solid phase only two very broad lines can be identified at frequencies ν_{12} = 148 MHz and ν_{34} = 252 MHz, giving $A_\mu(s\text{-Bu})$ = 400 MHz. These lines are much sharper and more prominent in the liquid phase, giving $A_\mu(s\text{-Bu})$ = 393 MHz at 92 K. An additional pair of much weaker lines is seen at 166 and 266 MHz in the liquid, possibly arising from the *n*-butyl radical, giving $A_\mu(n\text{-Bu}) \sim 432$ MHz.

There are two other much weaker, but arguably still clear, FT lines seen in the bottom (92 K) spectrum of Figure 1, at 166 and 266 MHz, both shifted up from those for the dominant *sec*-butyl radical by the same amount, giving a muon Hfcc of 432 ± 4 MHz. Similar FT-μSR spectra were also observed in the liquid phase at 225 and 250 K, but not in the solid where the FT lines are far too broad to reveal such weak transitions. As addressed more below, these lines are likely the corresponding ν_{12} and ν_{34} frequencies for the muoniated *n*-butyl radical.

Example ALC-μSR spectra, recorded over a range of temperatures, are shown by the example (background-corrected) Lorentzian fits to the data in Figure 2 at 60 and 80 K in the solid and in the liquid phase at 92 K (as in Figure 1), 175 and 250 K. (Note the *x*-axis

Table 1. Muon and β-Proton Hfcc for the *sec*-Butyl Radical Formed from 1-Butene

T (K)	A_μ [a]	A'_μ [a]	A_{p,CH_2} [b]	A_{p,CH_2Mu} [b]
10	461(4)[c]	145(2)	129(6)[c]	
30	460(4)[c]	144(2)	126(5)[c]	
60	430(4)	134(2)	107(6)	40(6)
80	398(3)	126(2)	105(4)	52(7)
92	393(1)	123.5(5)	90(3)	49(2)
125	369.0(8)	116.0(5)	83.3(5)	52.1(5)
150	353.8(5)	111.0(3)		
175	341.5(5)	107.2(3)	77.2(5)	56.5(5)
200	331.8(5)	104.2(3)	74.9(5)	57.8(5)
225	322.8(5)	101.4(3)	73.0(5)	58.9(5)
250	315.8(5)	99.2(3)	71.8(5)	60.3(5)

[a] Errors given in parentheses, with the minimum error assessed as ±0.5 MHz with the corresponding minimum error for $A'_\mu(T)$ set to be ±0.3 MHz. [b] The Δ_0 resonance for the eclipsed methylene protons are seen as a shoulder on the side of the strong Δ_1 line, but the staggered protons of $-CH_2Mu$ are well resolved at higher fields (Figure 2). [c] Very broad line fit to a single Δ_1 peak consistent with a shoulder Δ_0 resonance for the methylene protons.

scale change for the magnetic field range between the liquid and solid phases.) Like the FT data, the Δ_1 ALC lines are particularly broad in the solid phase (≳2000 G), partly due perhaps to the nonplanar nature of the dominant gauche conformer of 1-butene (paper I), giving rise to a more polycrystalline environment and hence to a larger expected hyperfine anisotropy.[30,31,33] This could also explain the broad FT lines seen in Figure 1 (top).

However, part of the line broadening seen in the neighborhood of the Δ_1 resonance at low temperatures is due to a shoulder Δ_0 resonance from the β-methylene ($-CH_2$) protons of the *sec*-butyl radical, which can be seen from the fits in the top two spectra in Figure 2. The strong Δ_1 minima at 15.7 kG at 60 K and 14.6 kG at 80 K give the muon Hfcc $A_\mu(s\text{-Bu})$= 426 ± 3 and 396 ± 2 MHz from eq 4, respectively, the latter in good agreement with the value found from the FT spectrum in Figure 1 above. The shoulder Δ_0 CH_2 resonances at 17.0 and 15.5 kG from the fits at these temperatures give the proton Hfcc A_{p,CH_2}= 106 ± 5 MHz at 60 K and 105 ± 4 MHz at 80 K from eq 5. Less convincing fits to this doublet were obtained at 10 and 30 K where this shoulder Δ_0 resonance was barely resolved.

The upper resonance seen at 20.7 kG at 60 K in Figure 2 is a second Δ_0 line, in this case from the β-protons of the $-CH_2Mu$ group, giving A_{p,CH_2Mu} = 39 ± 5 MHz. Similarly so for the spectrum at 80 K, giving A_{p,CH_2Mu} = 51 ± 6 MHz. These $-CH_2Mu$ resonances are off the scan ranges at the two lowest temperatures of 10 and 30 K. Averaged values of both muon and proton Hfcc for the muoniated *sec*-butyl radical from different determinations at a given temperature are also given in Table 1.

Since the ALC-μSR (Figure 2) spectra for the Δ_1 resonances of the muoniated *sec*-butyl radical seem unusually broad in the solid phase, even accounting for the aforementioned shoulder Δ_0 line, it raises the question of whether the ALC line shapes, assumed to be Lorentzian, may actually be due to an axial hyperfine tensor. Line shapes of this nature have mainly been investigated for the Mu−cyclohexadienyl radical in zeolites[31,33] and in soft matter[10] but also for the muoniated ethyl radical in zeolites.[11] However, fitting these data for the Δ_1 resonance with the assumption of an axial tensor at 10 and 60 K gave noticeably worse fits in the region of the minimum

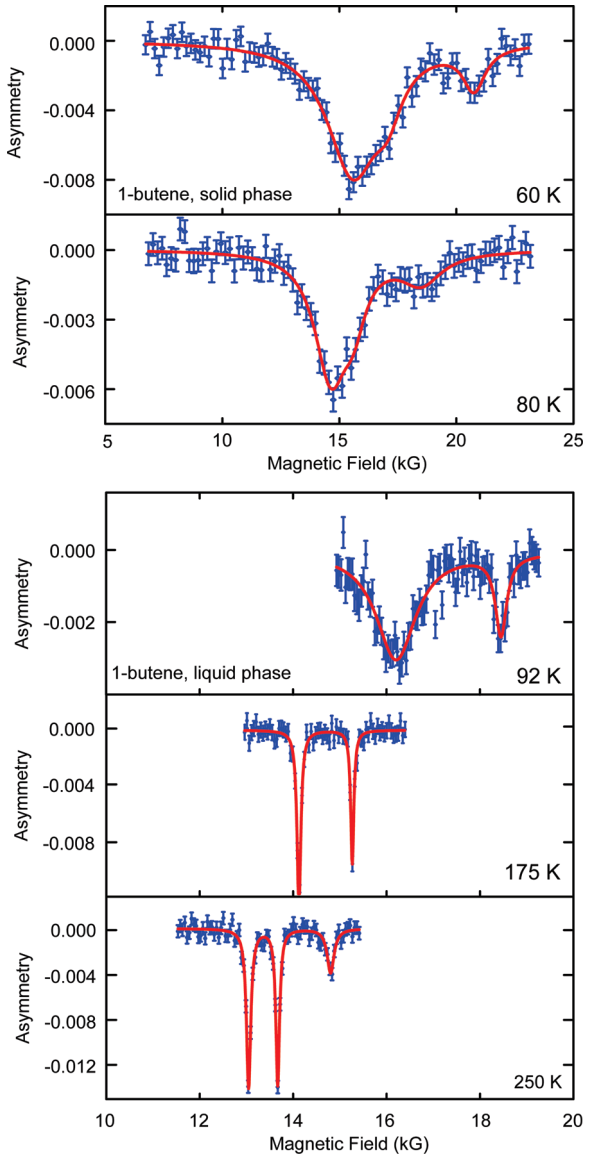

Figure 2. Representative ALC-μSR plots with Lorentzian fits for muoniated *sec*-butyl radicals formed from Mu addition to 1-butene, at temperatures of 60 K (top) and 80 K in the solid phase, and 92 K (just above the neat melting point of 88 K), 175 K, and 250 K in the liquid phase. Note the change in the scan range for the magnetic field in the liquid phase. At both 60 and 80 K a broad Δ_1 resonance is seen at the minimum with a shoulder Δ_0 resonance arising from the methylene protons. The higher field resonance at 60 and 80 K is also Δ_0, for the $-CH_2Mu$ protons. Just above the melting point, at 92 K, the Δ_1 resonance has predictably disappeared, leaving these same two Δ_0 lines, which are still broad. At the higher temperatures of 175 and 250 K in the liquid phase (lower scans), these lines are much sharper and shifted to lower fields (lower resonance, $-CH_2$; higher resonance, $-CH_2Mu$). A third weaker resonance seen clearly at 250 K at higher field (bottom scan) is probably a further Δ_0 line but is unidentifed.

compared to the Lorentizan fits shown. A high degree of hyperfine anisotropy was naturally indicated, though.

The Δ_1 resonance has predictably disappeared in the liquid phase, exemplified by the three lower spectra in Figure 2. At 92 K, the same two Δ_0 resonances for the muoniated *sec*-butyl radical as seen in the solid phase are apparent, with A_{p,CH_2} = 90 ± 2 MHz and A_{p,CH_2Mu} = 49 ± 2 MHz, from the lower and upper

dx.doi.org/10.1021/jp109676b |J. Phys. Chem. A 2011, 115, 2778–2793

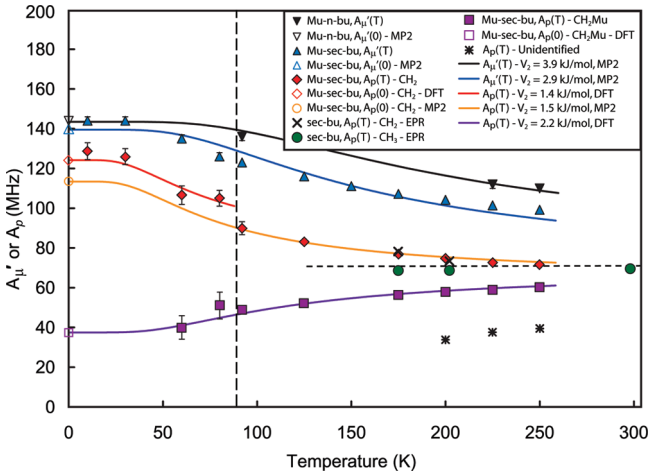

Figure 3. Temperature dependences for the reduced muon, $A'_\mu(T)$, and proton, $A_p(T)$, Hfcc for predominantly the *sec*-butyl radical formed from Mu addition to 1-butene. The blue triangles and fitted cyan trend (MP2 calculations of paper I) are for $A'_\mu(T)$, while the red diamonds and red and orange fitted trend lines are B3LYP and MP2-calculated fits for $A_{p,CH_2}(T)$ in the solid and liquid phases, respectively. The solid magenta squares and fitted trend line are the data and B3LYP-calculated Hfcc for the staggered protons, $A_{p,CH_2Mu}(T)$. The black asteriks are proton Hfcc from assumed Δ_0 resonances at high fields and are unidentifed. The vertical dashed line at 88 K is the melting point of neat 1-butene. The three upper-most inverted (black) triangles and MP2-calculated fitted trend for $A'_\mu(T)$ are for a tentative indentification of the primary *n*-butyl radical. Also shown are EPR data points for the methylene protons (black crosses) and for the terminal methyl group (solid green circles) of the unsubstituted *sec*-butyl radical. The dashed black line is the calculated high-temperature limit. The fitted torsional barriers from the colored trend lines shown are given in the legend. Several (unfilled) theory points plotted for calculated Hfcc at 0 K along with the calculated trend lines are discussed in the text.

resonances, respectively, which are still surprisingly broad at this temperature. (This might be due to some incomplete melting in the polycrystalline environment of 1-butene.) At higher temperatures, seen in the scans at 175 and 250 K, both of these Δ_0 resonances are much sharper and more pronounced, as is typically the case in liquids, and are shifted to lower fields. In addition, at the highest temperature of 250 K (bottom), there is a third, weaker, resonance near the end of the scan, but which is nevertheless clearly seen. Similar spectra were seen at 200 and 225 K in the liquid phase, but this high-field resonance is outside the scan range at lower temperatures. This weak line is probably another Δ_0 resonance but remains unidentified. The proton Hfcc for the three Δ_0 resonances seen at 250 K in Figure 2, in the order shown, are A_{p,CH_2} = 71.8 ± 0.5 MHz, A_{p,CH_2Mu} = 60.3 ± 0.5 MHz, for the *sec*-butyl radical, as recorded in Table 1, and A_p = 40 ± 1 MHz, for the unidentified radical. The intensities of the two strong lines seen are equal, consistent with their origin.

The muon Hfcc, expressed in reduced form, $A'_\mu(T)$, along with the two dominant β-proton Hfcc of the *sec*-butyl radical identified above, $A_{p,CH_2}(T)$ and $A_{p,CH_2Mu}(T)$, reported in Table 1, are plotted in Figure 3, which also plots the data for $A'_\mu(T)$ for what may be the muoniated *n*-butyl radical (inverted solid black triangles), along with the proton Hfcc for the unidentified weak Δ_0 resonance seen at the high fields, noted above.

The $A'_\mu(T)$ data for the *sec*-butyl radical follow a smooth trend from the solid to the liquid phase (blue triangles in Figure 3), with no obvious gap at the 1-butene melting point (88 K, vertical dashed line), in marked contrast to the discontinuity seen for Mu−*tert*-butyl reported in ref 7 (see also Figure 7 below) and for the *sec*-butyl isomers formed from 2-butene (Figure 6 below). However, given the inherent scatter in the data, a consequence of the broad nature of the FT and ALC lines discussed above, and the possibility that additional conformers (paper I) may be contributing here, along with the fact that there are only two data points near the phase transition, a small gap at the transition temperature cannot be totally ruled out. The blue trend line here is a fit of the $A'_\mu(T)$ data to the model of eq 10 discussed later. The upper black fitted line to the inverted triangles assumes formation of the *n*-butyl radical, and is also discussed below.

The solid red diamonds in Figure 3 are the data for the methylene protons, $A_{p,CH_2}(T)$, with the red and orange trend lines fits to these data in the solid and liquid phases, respectively, also to the model of eq 10 discussed below. Though not dramatic, there does appear to be a real discontinuity seen in $A_{p,CH_2}(T)$ at the melting point of 1-butene (88 K), which is outside the scatter in the data, and consistent with the separate fit lines shown. The data for the protons of $-CH_2Mu$, $A_{p,CH_2Mu}(T)$, are shown by the solid magenta squares and fitted trend line. The back asterisk points plotted at the bottom of the figure are the proton Hfcc for the unidentified more weakly formed (Δ_0) resonance seen.

Also shown in Figure 3 are two sets of β-proton Hfcc for the *un*substituted *sec*-butyl radical from early EPR studies,[2,4] for the methylene protons (black crosses), which fall on the same fitted (orange) trend line as the μSR data for $A_{p,CH_2}(T)$ in the liquid phase, and for the protons of the terminal methyl group (solid green circles), showing temperature-independent methyl proton Hfcc. The fitted orange trend line for $A_{p,CH_2}(T)$ merges with the dashed black line from theory, discussed below.

3.2. Mu−*sec*-Butyl Radicals from *cis*- and *trans* 2-Butene. In contrast to 1-butene, only one structural isomer is possible for the muoniated radical formed from Mu addition to 2-butene, the *sec*-butyl radical with the structural formula $CH_3CHMu\dot{C}HCH_3$. However, from Mu addition across the double bond, distinct *cis*- and *trans*-*sec*-butyl radicals are formed in the solid phase that reflect the geometries of the parent butenes, as the Hfcc data in Figure 6 below show. The muon is placed at the central methylene (−CHMu) position, in contrast to both *tert*-butyl[7] and *sec*-butyl from 1-butene discussed above, where it is placed in the terminal methyl group, $-CH_2Mu$. As previously, both TF/FT-μSR and ALC-μSR spectra were recorded and analyzed to yield the muon and proton Hfcc of interest. Typical FT-μSR spectra in the solid phase are shown in Figure 4 for the cis radical at 20 K (top) and for the trans radical at 25 K (bottom). The structures of the separate cis and trans radicals are shown by the insets. These FT lines are much sharper than in the 1-butene case (Figure 1, top), suggesting a more single-crystal-like environment for 2-butene, with a reduced degree of hyperfine anisotropy, compared to that for 1-butene. The sum of the two radical frequencies ν_{12} and ν_{34} seen again gives the muon Hfcc, A_μ(cis) = 469 ± 1 MHz and A_μ(trans) = 449 ± 1 MHz at these temperatures, both in good agreement with fits to the TD data for $A(t)$ from eq 1 and generally also in good agreement with the values determined from ALC fits to the positions of the Δ_1 level crossing resonances. See entries in Table 2.

Representative ALC-μSR spectra for the *sec*-butyl radical formed from *trans*-2-butene are shown in Figure 5, at 75 and 100 K in the solid phase and at 170 K (just above the neat melting point of 168 K), 200 K, and 250 K in the liquid phase. As in Figure 2, the fitted lines are to Lorentzian line shapes from background-corrected ALC spectra. In the solid phase (top two spectra), a clearly resolved doublet of a strong Δ_1 resonance at lower fields for the muon Hfcc of

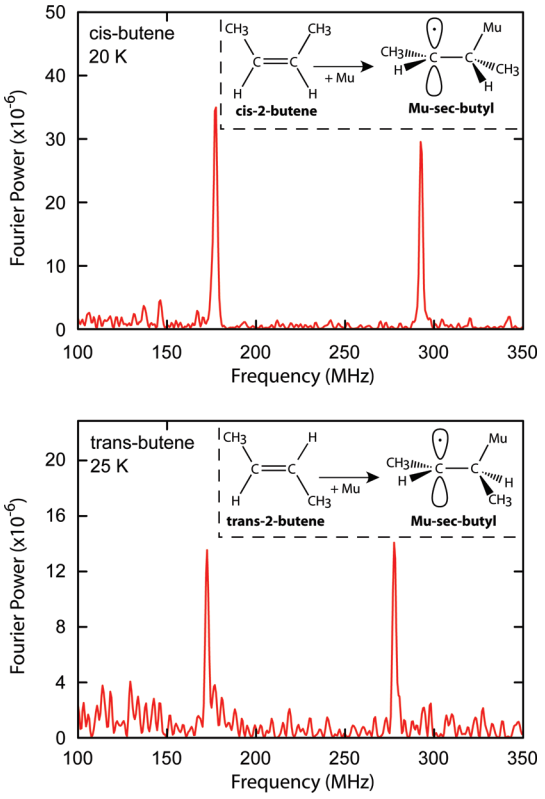

Figure 4. Example FT-μSR spectra in the solid phase for the *sec*-butyl radicals formed from Mu addition to *cis*-2-butene at 20 K (top) and to *trans*-2-butene at 25 K (bottom), at a field of 3.80 kG. The insets show the separate geometrical structures for the *cis*- and *trans*-2-butyl radicals formed. These FT lines are surprisingly sharp in comparison with similar data for the *sec*-butyl radical formed from Mu addition to 1-butene (Figure 1, top). The strong lines seen are the ν_{12} and ν_{34} transitions for the *sec*-butyl radicals formed, the sum of which gives the isotropic muon Hfcc, A_μ(cis) = 468 MHz and A_μ(trans) = 450 MHz at these temperatures. See entries in Table 2. The diamagnetic frequency, ν_D, is off scale in both plots.

−CHMu is seen, exemplified by the peak at 16.4 kG in the 75 K scan (giving a muon Hfcc A_μ = 446 MHz), along with a nearby Δ_0 resonance at 17.2 kG attributed to the eclipsed protons of the terminal CH_3 group (A_{p,CH_3} = 122 MHz). This doublet could be resolved down to the lowest temperature of 25 K, in contrast to the data for 1-butene in Figure 2. A further Δ_0 resonance is seen at 20.1 kG at 75 K, due to the β-proton of the −CHMu group (with $A_{p,CHMu}$= 67.5 MHz). The ALC line widths in the solid are also relatively narrow here ($\lesssim$1000 G), consistent with a reduced degree of hyperfine anisotropy. The intensities (peak areas) of the $A_{p,CH_3}(T)$ and $A_{p,CHMu}(T)$ level crossings in the solid are qualitatively consistent with an expected ratio of 3:1 from the assignments noted above.

In the liquid phase (bottom three spectra in Figure 5), the Δ_1 resonance has again disappeared, leaving the same two Δ_0 resonances corresponding to $A_{p,CH_3}(T)$ and $A_{p,CHMu}(T)$, which are much sharper ($\lesssim$50 G) than in the solid, even just above the melting point (middle scan), in clear contrast as well to the broad lines seen just above the 1-butene melting point in Figure 2. In like manner though they also shift to lower fields at higher temperatures. Even so these lines from *trans*-2-butene remain partially merged at both 170 and 200 K and have collapsed completely into a single line by 225 K, indicating opposite *T*-dependences, as seen in the scan at 250 K shown at the bottom of Figure 5. The intensity ratio for this partially resolved pair of Δ_0 lines in the liquid is a bit puzzling though, more like 1/1 rather than the expected ratio of 3/1 inferred from the solid phase. This could be an artifact of these narrow lines having widths comparable to the step sizes in the ALC scans carried out. There are no other assignments consistent with the data. Only two Δ_0 resonances could be consistently identified, with their proton Hfcc recorded in Table 2.

ALC-μSR spectra were also taken for the *sec*-butyl radical formed from *cis*-2-butene, over a temperature range similar to that in the *trans*-2-butene case, revealing a similar doublet at low temperatures, with a Δ_0 resonance also attributed to the eclipsed protons of the terminal CH_3 group again appearing on the side of the strong Δ_1 resonance, giving similar proton Hfcc at low temperatures. However, in contrast to the trans radical, this was much more weakly developed and could only be identified at 7 K (giving A_{p,CH_3}= 128 ± 2 MHz) and 20 K (A_{p,CH_3}= 127 ± 2 MHz), before being lost in the tail of the much stronger Δ_1 resonance at higher temperatures, an effect that was exacerbated by shifting backgrounds in these particular data. The Δ_0 resonance due to the −CHMu group was much more distinctly seen though, up to 150 K. At the highest temperatures, only a single broad line was observed, possibly due to residual O_2 in this sample, from which reliable proton Hfcc could not be determined. The data for the proton Hfcc of the −CHMu group of the cis radical, along with that for the corresponding muon Hfcc seen over a wider temperature range, are also recorded in Table 2.

Table 2. Muon and β-Proton Hfcc for the *sec*-Butyl Radicals Formed from *cis*- and *trans*-2-Butene

	cis-2-butene			*trans*-2-butene			
T (K)	A_μ [a]	A'_μ [a]	$A_{p,CHMu}$ [b]	A_μ [a]	A'_μ [a]	A_{p,CH_3} [c]	$A_{p,CHMu}$ [b]
7	469.5(5)	147.4(5)	68(2)				
10				450(2)	141.3(10)		
20	468(1)	147(1)	69(2)				
25				450(1)	141.3(6)	125.4(20)	
40	468.0(5)	147.0(5)	68.4(8)				
50				448.5(10)	140.9(8)	124.2(10)	66(2)
60	461(1)	145(1)					
75				444.0(5)	139.5(3)	122.8(8)	67.6(8)
80	451.2(5)	141.6(3)	68.4(10)				
100	436.8(5)	137.1(3)	66.5(6)	438.5(15)	137.7(10)	119(1)	68(2)
110	428.3(5)	134.5(3)	68.0(5)				
120	419.1(5)	131.6(3)	68.4(8)				
131	409.0(5)	128.4(3)	68.5(6)				
134	370.4(5)	116.3(3)	69.5(10)				
137	368.7(5)	115.8(3)	67.7(6)				
150	361.8(8)	113.6(6)	68(2)	410.5(5)	128.9(3)	113.4(10)	
165				399(2)	125.3(10)	113(3)	
170	351.8(6)	110.5(4)		352.5(10)	110.7(5)	72.4(10)	68.3(10)
180				347.6(5)	109.2(3)	71.5(6)	68.2(6)
200	338.8(6)	106.4(3)		338.6(5)	106.3(3)	70.5(6)	68.2(6)
225	328.0(10)	103(1)		328.5(10)	103.2(6)		68.8(10)
250	320(2)	100.5(15)		319.2(5)	100.2(3)		68.4(10)

[a] Errors given in parentheses, with the minimum error assessed as ±0.5 MHz with the corresponding minimum error for $A'_\mu(T)$ set to be ±0.3 MHz. [b] Staggered proton Hfcc for both the *trans* and *cis*-2-butyl radicals. [c] Proton Hfcc for the terminal methyl group is from a clearly resolved doublet consistently seen for the *trans*-2-butyl radical (Figure 5) but not so for the *cis*-2-butyl radical, as discussed in the text.

dx.doi.org/10.1021/jp109676b |*J. Phys. Chem. A* 2011, 115, 2778–2793

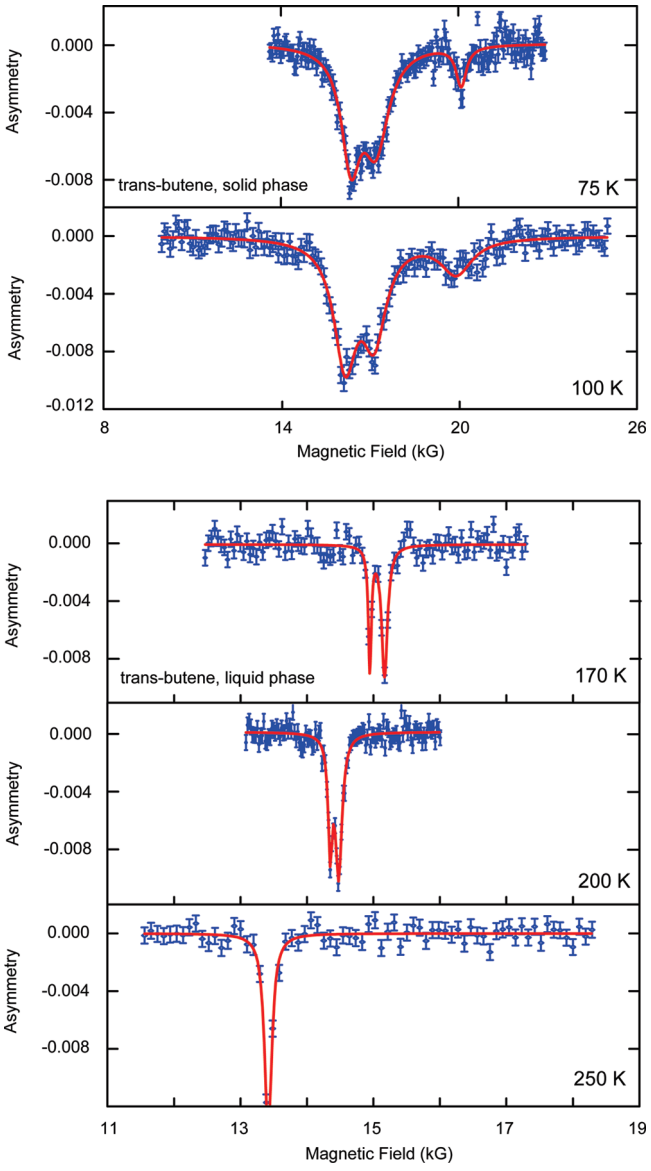

Figure 5. Representative ALC plots for the *sec*-butyl radical formed from Mu addition to *trans*-2-butene, at 75 K (top) and 100 K in the solid phase and in the liquid phase at 170 K, just above the 168 K neat melting point (middle scan) and at 200 and 250 K (bottom scan). Note the scale change for the magnetic field range for the liquid-phase data. As in Figure 2, the solid lines shown are Lorentzian fits to background-corrected data. In the solid phase the strong resonance at the lowest fields is the Δ_1 line for the muon Hfcc of the −CHMu group, with the nearby resonance a Δ_0 line for the methyl protons. The upper resonance is also a Δ_0 line but for the single proton of −CHMu. In the liquid phase (bottom three scans), the Δ_1 resonance has disappeared, leaving these same two Δ_0 resonances, but which are much sharper and also overlap at the highest temperatures. See entries in Table 2 and discussion in the text.

The muon and proton Hfcc $A'_\mu(T)$, $A_{p,CH_3}(T)$ and $A_{p,CHMu}(T)$ at different temperatures, for both the muoniated cis and trans radicals formed from their parent 2-butenes, reported in Table 2, are plotted in Figure 6. Like similar data from 1-butene in Table 1, these Hfcc are averaged values from variations in the method of analysis and include as well estimates of systematic error from different beam periods. As in Figure 3, a number of theory points at 0 K as well as colored trend lines, mainly from fits to model calculations of the T-dependences for $A'_\mu(T)$ and $A_p(T)$

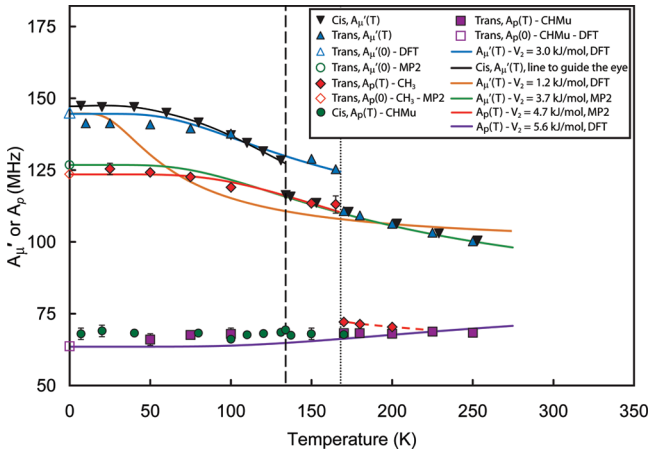

Figure 6. Temperature dependences for the Hfcc $A'_\mu(T)$ and $A_p(T)$ for the *sec*-butyl radicals formed from *cis*- and *trans*-2-butene. The inverted black triangles and guideline to the eye are $A'_\mu(T)$ for the *cis*-butyl conformer while the blue triangles and fitted trend line are for the trans conformer. (The cis points in the liquid have been shifted up by 3 K for clarity.) Noteworthy are the distinct discontinuities seen in $A'_\mu(T)$ for both the cis (134 K, vertical dashed line) and trans (168 K, vertical dotted line) conformers at their respective bulk melting points. The solid orange line is a B3LYP calculation for the *trans*-butyl muon Hfcc in the liquid phase, discussed in the text. The red diamonds and fitted red trend line are the β-proton Hfcc for the CH_3 group of *trans*-2-butyl, $A_{p,CH_3}(T)$, in the solid phase. The dramatic discontinuity seen in $A_{p,CH_3}(T)$ (broken red guideline) at the phase transition is also noteworthy. The lower data points are the staggered proton Hfcc of the −CHMu group for both the *cis*- (solid green circles) and *trans*-butyl (magenta squares) conformers, which are essentially indistinguishable by experiment. The magenta trend line is a fit for the B3LYP-calculated proton of −CHMu for the *trans*-butyl radical. Note the lack of any discontinuity in these −CHMu proton Hfcc at the neat melting points. A number of calculated Hfcc are shown at 0 K (unfilled points) and these, along with the fitted trend lines, are discussed in the text.

discussed below, are shown. Some remarks though are worth making at this time.

First, at the lower temperatures in the solid phase, the muon Hfcc $A'_\mu(T)$ from −CHMu formed from *cis*-2-butene (solid black inverted triangles and guideline to the eye) are about 6 MHz higher than from the trans isomer (blue triangles and fitted trend line), but in the liquid phase they are identical (the cis points have been slightly shifted for clarity). The different Hfcc seen in the product *cis*- and *trans*-2-butyl radicals indicates preservation of the geometry of the parent isomers in the solid phase. Both isomers exhibit a sharp discontinuity in $A'_\mu(T)$ at their respective bulk melting points (134 K for cis, vertical dashed line and 168 K for trans, dotted line). The marked decreases seen in muon Hfcc at the separate phase transitions are similar to the behavior reported for Mu−*tert*-butyl in ref 7, which is plotted also in Figure 7 below, but contrast sharply with the continuous dependence seen for *sec*-butyl from 1-butene in Figure 3.

Second, the large and slowly varying values of $A_{p,CH_3}(T)$ for the proton Hfcc of the terminal CH_3 group of the *trans*-butyl radical in the solid phase, seen in its shallow T-dependence and hence broad plateau in Figure 6 (red diamonds and fitted trend line), indicates a high torsional barrier. This seems surprising on the surface, in view of what appears to be a general expectation that the proton Hfcc of terminal methyl groups would be T-independent, seen for the *tert*-butyl radical in ref 7, for the unsubstituted *sec*-butyl radical in Figure 3, and for the unsubstituted ethyl radical (see ref 11). In all of these cases only a small torsional barrier is indicated over measured temperature

dx.doi.org/10.1021/jp109676b |J. Phys. Chem. A 2011, 115, 2778–2793

ranges. The methyl proton Hfcc for *trans*-2-butyl here also exhibits a *huge* discontinuity at the neat melting point, similar to but even more dramatic than that exhibited by both $A'_\mu(T)$ and $A_{p,CH_2}(T)$ for the methylene protons in *sec*-butyl from 1-butene in Figure 3. To our knowledge, neither such large experimental proton Hfcc near 0 K nor such clear discontinuities in $A_p(T)$ have previously been reported in alkyl radicals, from either μSR or EPR studies.

Third, the temperature dependence for the staggered proton Hfcc of the single proton of the −CHMu group, $A_{p,CHMu}(T)$, for both the cis and trans isomers is essentially the same, as shown by the lower solid green circles (cis) and magenta solid squares (trans) and fitted (magenta) trend line to the *trans*-butyl data in Figure 6. Not only the calculated results but also the opposite temperature dependences seen experimentally clearly identify these two different proton environments. It is noteworthy that, in contrast to $A_{p,CH_3}(T)$, there is *no* discontinuity in $A_{p,CHMu}(T)$, for either the *cis*- or *trans*-2-butyl radicals at their respective melting points, a situation that also prevails for the proton Hfcc of $-CH_2Mu$ in the *sec*-butyl radical from 1-butene (Figure 3), and for the same group in the muoniated ethyl radical.[11,14]

4. ASPECTS OF THEORY

4.1. Synopsis of Calculations in Paper I. Two theoretical approaches have been implemented for geometry optimization and the calculation of Hfcc within the BO approximation in paper I: a hybrid DFT method with the B3YLP density functional and an EPR-III basis set, implemented in Gaussian03, and at the spin-unrestricted MP2 (UMP2) level of theory, with the same EPR-III basis set. All Hfcc are single molecule calculations, i.e., are calculated in vacuo at 0 K. A simple approach to approximately account for vibrational corrections to Hfcc calculations[19,25,35−38] was implemented, in which the C−Mu bond length was stretched slightly to 1.07 times the equilibrium C−H bond distance, determined from the calculations of Bohm et al. for the muoniated ethyl radical,[25] and Hfcc calculations carried out on this modified but static geometry. A similar scale factor can be found in the calculations of Webster and Buttar[19] and of Claxton et al.,[38] also for the Mu-substituted ethyl radical.

4.2. *T*-Dependences of β-Hfcc: Barriers to Internal Rotation. For all C−Mu bonds in muoniated alkyl radicals, $A'_\mu(T)$ decreases with increasing temperature. This is in accord with the accepted view, also discussed in paper I, that the C−Mu bond in the β position to the radical center is at a potential minimum and "eclipses" the electron p_Z orbital, resulting in a maximum Hfcc at 0 K,[7,12,14,16,18,26] and which also reflects the effects of vibrational averaging.[14,16,19,25,36,38] With increasing temperature, enhanced vibrational motion of the C−Mu bond facilitates excursions away from 0° and results in the muoniated alkyl group rotating away from this favored conformation, about the $C_\alpha-C_\beta$ bond axis, thereby decreasing the electron spin density at the muon and hence its Hfcc, $A'_\mu(T)$. Concomitantly, the "staggered" protons in the same group as the muon, exemplified by the common case of $-CH_2Mu$, exhibit the opposite dependence, with $A_{p,CH_2Mu}(T)$ increasing with increasing temperature. This *T*-dependence provides a ready measure of the barrier to internal rotation for Mu-substituted alkyl groups.

For β-substituted alkyl radicals, the torsional barrier to hindered rotation, V_B, is defined by the potential difference between conformations of maximum and minimum energy,

$$V_B = [V_{Eff}(\theta_1)]_{max} - [V_{Eff}(\theta_2)]_{min} \quad (6)$$

where θ_1 and θ_2 are the corresponding dihedral angles for internal rotation and where $V_{Eff}(\theta)$ depends on both electronic and ZPE contributions. For isotopically substituted radicals, within the BO approximation, differences in barrier heights will be solely due to differences in ZPEs, which are expected to be largest for muoniated radicals due to the effect of the light muon mass on specific vibrational modes. However, large barriers to internal rotation can also be expected for specific eclipsed C−H bonds, alluded to above and confirmed below for the *sec*-butyl radicals in this study.

As commented at the outset, there have been several theoretical calculations of torsional barriers for alkyl radicals, for the *un*substituted ethyl,[16,39] propyl,[18] and *tert*-butyl[21] radicals. Calculated barrier heights for methyl rotation vary from ∼100 to 300 J/mol for the ethyl radical,[16,17,39] with coupling to torsional modes also affecting this barrier height,[39] to ∼400 J/mol for the propyl radical, to as high as ∼5 kJ/mol from earlier SCF calculations for the *tert*-butyl radical.[21] Carmichael has also carried out similar calculations (unpublished) for unsubstituted butyl radicals, finding barriers for methyl rotation in *tert*-butyl of ∼3.5 kJ/mol and in *sec*-butyl of ∼2 kJ/mol.[40] For the *muoniated* ethyl radical, V_B is ∼1.9 kJ/mol from the calculations of Claxton and Graham[16] and similarly so for muoniated *n*-propyl,[18] both much higher than for the unsubstituted radicals, reflecting the expected ZPE enhancements noted earlier.

A phenomonological and now classic approach to evaluate the barrier to internal rotation for β-protons in alkyl radicals was established by Fessenden,[1] in which the intramolecular torsional potential is assumed to have 2-fold angular symmetry for a pair of rigidly rotating alkyl groups about the $C_\alpha-C_\beta$ bond axis, of the form

$$V_2(\theta) = \frac{1}{2}V_2(1 - \cos 2\theta) \quad (7)$$

ignoring molecular vibrations about the minimum[39] as well as host−guest or solvent interactions, and which has been widely employed over the years in both EPR[1,3,5,12] and μSR[7,12,16] studies. The barrier height V_2 is defined by the difference between eclipsed ($\theta = 0°$) and staggered ($\theta = 90°$) conformations, though in the present study this is found from staggered bonds near ±120°. In accord with the 2-fold symmetry of the potential, and the implied assumption of a planar radical, eq 7 also implies symmetry about p_Z for $\pm\theta$ rotations, which is not strictly true for the muoniated *sec*-butyl radicals of interest here.

Other potential forms for $V_B(\theta)$ have also been considered to better represent the dihedral angle dependence of the torsional surface. For alkyl radicals the generic group of interest is a terminal CH_3 group, suggesting a potential of the form $V_3(\theta) = {}^1/_2V_3(1 - \cos 3\theta)$, reflecting equal interaction minmima at 0° and ±120° for a rotating CH_3 group. Such a potential is found to describe the torsional surface for the unsubstituted *tert*-butyl radical from the SCF calculations of ref 21, even with nonplanar symmetry, and has been considered by Percival et al. for the muoniated *tert*-butyl radical,[7] and more recently by Shiotani et al. for some dimethyl ether radical cations[41] and implicitly by McKenzie et al. for the Mu adduct of diketene.[32] The potential function $V_6(\theta) = {}^1/_2V_6(1 - \cos 6\theta)$, or variations of it, is also well-known in the literature,[7,41,42] and more completely reproduces the natural 6-fold symmetry of an *un*substituted β-methyl group. On the other hand, for the *substituted* β-methyl group, notably here $-CH_2Mu$, but also for the methylene protons of CH_3CH_2-, the inherent 6-fold torsional symmetry of unsubstituted methyl is approximately reduced to the 2-fold potential of eq 7, which has been assumed for all the muoniated butyl radicals in the present study.

Different rotational conformers will have different Hfcc, $a_j(\theta_j)$, and if the interchange rate beteween these conformers is larger than

the differerence between Hfcc, a mean value for the β-Hfcc will be observed at temperature T, defined by

$$\langle A_\beta \rangle(T) = (\sum_j a_j e^{-E_j/k_B T})/(\sum_j e^{-E_j/k_B T}) \quad (8)$$

with probabilities given by a Boltzmann distribution, here with energies E_j given by the torsional potential of eq 7. An early example of the use of of eq 8 in studies of butyl radicals was given by Krusic et al.[3] who fit their EPR data using INDO-calculated values of proton Hfcc, finding barrier heights V_2 for the isobutyl and *n*-propyl radicals to be 1.2 and 1.7 kJ/mol, respectively, comparable to those cited above.

A similar approach was taken by Ramos et al.[12] and by Percival et al.[7] in early μSR studies of the muoniated ethyl and *tert*-butyl radicals, respectively, also using the 2-fold potential of eq 7. These authors carried out a more rigorous calculation by solving the torsional Hamiltonian for the energy levels E_j, but assumed the phenomonological McConnell form[3,7,42] of the β-muon Hfcc in doing so,

$$a_j(\theta_j) = L + M\langle \cos^2(\theta \pm \theta_0)\rangle_j \quad (9)$$

where θ_0 is the value of the dihedral angle θ at the potential minimum. Hyperconjugation effects (delocalization of the spin density) depend on geometry and are largely reflected in the value of M whereas the L parameter is primarily a measure of orientation-independent mechanisms, such as spin polarization ($L \ll M$). From fits to the experimental T-dependence of the muon Hfcc, Ramos et al.[12] determined the barrier height for muoniated ethyl to be V_2 = 2.8 kJ/mol in the liquid phase, higher than from ab initio calculations.[16] Percival et al. found V_2 = 3.4 kJ/mol for muoniated *tert*-butyl in the solid phase, with V_2 = 2.1 kJ/mol in the liquid phase, with some variation depending on parameter changes. These barrier values are relevant to the discussion that follows.

Our approach here is also predicated on eqs 7 and 8, where the Hfcc $a_j(\theta_j)$ are assumed to be given by those calculated at 0 K at potential minima of 0° and (near) ±120° from the B3LYP or MP2 calculations of paper I, with the energies E_j found from eq 7 at these angles. From such a simple model, selecting just three equilibrium angles, we cannot expect to achieve more than a *qualitative* understanding of the role of the torsional barrier height in dictating the observed T-dependence for $A_\beta(T)$ for the muoniated butyl radicals of interest, but it has the great advantage of being computationally simple and physically transparent. It should be noted that the specific Hfcc, $a_j(\theta_j)$, are assumed to be T-independent. Changes in $a_j(\theta_j)$ due to changes in environment can be expected to be at the few percent level,[20,25,32,35,43] except in the case of supercritical environments.[14]

Though eq 8 is inherently a high-temperature approximation, where the assumption of fast exchange between different conformers is best satisfied, in practice it gives good fits to data for both $A'_\mu(T)$ and $A_p(T)$ down to ~10 K, where Hfcc are dominated by near-constant values at 0 K (eq 9), in accord as well with similarly motivated fits to data for dimethylether cations reported by Shiotani et al.,[41] also down to similar low temperatures. The ESR study of ref 41 is in fact quite close in methodolgy to that of the present paper, in that molecular geometries and Hfcc were also found from both B3LYP and MP2 calculations. A somewhat related approach based on ZPE differences has been considered by McKenzie et al. in μSR studies of Mu addition to diketene[32] and for the muoniated methyl radical,[20] and by Cormier et al. for the muoniated ethyl radical in CO_2.[14]

It follows then, from eq 8 for *eclipsed* C−Mu (or C−H) bonds of the present study, that

$$\langle A_\beta \rangle(T) = \frac{[a(0) + (a(120) + a(-120)) \times e^{-(0.75V_2/k_B T)}]}{(1 + 2e^{-(0.75V_2/k_B T)})} \quad (10)$$

where, at the potential minimum, θ_0 = 0°, so $V_2(\theta{=}0) = 0$, otherwise $V_2(\theta{=}\pm120) = 0.75\ V_2$. On the other hand, for *staggered* conformations of C−H bonds,

$$\langle A_\beta \rangle(T) = \frac{[a(120) + (a(0) + a(-120)) \times e^{-(0.75V_2/k_B T)}]}{(1 + 2e^{-(0.75V_2/k_B T)})} \quad (11)$$

where now θ_0 is assumed to be 120°, so $V_2(\theta - \theta_0) = 0$, otherwise $V_2(\theta{=}0) = V_2(\theta{=}-120) = 0.75V_2$. Note, as $T \rightarrow \infty$ ($k_B T \gg V_2$), $A_\beta(T) \rightarrow {}^1/_3[a_\beta(0) + a_\beta(120) + a_\beta(-120)]$, for either the eclipsed or staggered conformations, giving the averaged T-independent "free rotor" limit expected at high temperatures.

When the present data for muoniated *sec*-butyl radicals are fitted to eq 10 or 11, the level of agreement between the calculated and experimental trends with temperature provides an assessment both of the calculated Hfcc reported in paper I and of the barrier to internal rotation. Despite the limitations of this simple model, and the assumed validity of the 2-fold potential of eq 7, on balance this approach gives a good account over the whole temperature range of both the measured muon and proton Hfcc for the muoniated *sec*-butyl radicals butyl radicals of interest here, including for terminal methyl groups. The fitted barriers (V_2) so determined are also in accord with those determined elsewhere for alkyl radicals by similar fitting procedures,[3,7,12] and in particular for $A'_\mu(T)$ from muoniated *tert*-butyl,[7] as discussed below.

5. DISCUSSION: HFCC FOR MUONIATED *SEC*-BUTYL RADICALS

The results for the T-dependences of the (reduced) muon, $A'_\mu(T)$, and proton, $A_p(T)$, Hfcc for the muoniated *sec*-butyl radicals of this study and their comparison with theory and with some EPR data are shown in Figures 3 and 6, which, along with Figure 7 for the muon Hfcc of the *tert*-butyl radical, provide the basis for the discussion that follows.

At low temperatures, near 0 K, where $\langle \cos^2 \theta \rangle$ in eq 9 does not differ appreciably from unity, we can expect $A'_\mu(T)$ to be $\sim L + M$ and hence remaining near constant at its maximum value for the eclipsed C−Mu bond in the "McConnell plateau" region. This is seen for all Mu−butyl radicals and is established for muoniated ethyl as well.[11] The observation of such slowly-varying muon Hfcc at low temperatures can be traced to relatively high (~3 kJ/mol) torsional barriers to internal rotation. Less well established is the similar T-dependence and plateau region also seen in the solid phase in the present study for proton Hfcc in *un*substituted alkyl groups, due to eclipsed C−H bonds and which also exhibit large torsional barriers, with Hfcc near 0 K comparable to those for $A'_\mu(0)$.

5.1. "Benchmark" Assessment of $A'_\mu(T)$ for *tert*-Butyl. A first assessment of the utility of the simple model of eq 10, using the calculated Hfcc of paper I to fit the data for $A'_\mu(T)$, is carried out for the muoniated *tert*-buyl radical, with the structural formula $(CH_3)_2\dot{C}CH_2Mu$, formed by Mu addition to isobutene. The calculated Hfcc are compared with the results of Percival et al.[7] and of Roduner et al.[22] but include as well three data points from the present study at temperatures below 50 K, as shown in Figure 7.

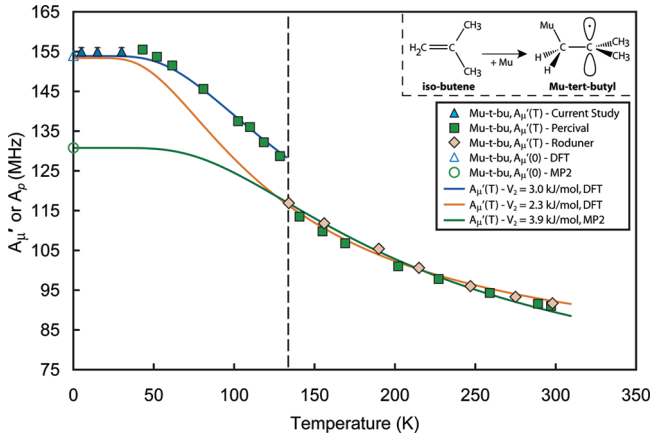

Figure 7. Temperature dependences for the muon Hfcc, $A'_\mu(T)$, for the muoniated *tert*-butyl radical, mainly from the data of ref 7 (green squares) and of ref 22 in the liquid phase (shaded brown diamonds) but including as well $A'_\mu(T)$ data from the present study at temperatures below 50 K (solid blue triangles). The inset shows the structure of the *tert*-butyl radical formed. The vertical dashed line denotes the melting point of neat isobutene, at 133 K. The sharp discontinuity in $A'_\mu(T)$ here is noteworthy. As in Figures 3 and 6, the colored trend lines are based on simple model calculations utilizing the calculated Hfcc from paper I and give different torsional barriers (see legend) and are discussed in the text. The calculated values at 0 K are shown by the unfilled points.

At 0 K, the B3LYP-calculated value for $A'_\mu(0)$ is 154 MHz from paper I (unfilled blue triangle) in seeming excellent agreement with the data. A fit of eq 10 to $A'_\mu(T)$ in the solid phase, from the B3LYP-calculated muon Hfcc shown by the blue line, also gives an excellent account of the trend with temperature up to the melting point, giving a fitted torsional barrier V_2 = 3.0 kJ/mol, with a few percent error, an equally good fit to that reported from the more sophisticated calculations of ref 7 that gave a very similar barrier (3.4 kJ/mol).

There is a marked discontinuity seen in $A'_\mu(T)$ at the 133 K melting point of isobutene in Figure 7. Thermal-average models represented by eq 8 cannot possibly account for such a discontinuity, which is a clear indication of environmental effects, either intramolecular or host−guest intermolecular (lattice) interactions on the muon Hfcc in the solid phase. A key question then is how to intrepret this discontinuity and, concomitantly, how best to describe the $A'_\mu(T)$ data in the liquid phase?

Percival et al.[7] obtained a good fit to $A'_\mu(T)$ for their liquid-phase data for muoniated *tert*-butyl assuming the same value for $A'_\mu(0)$ as in the solid, giving a fitted barrier height V_2 = 2.1 kJ/mol (somewhat dependent on assumptions). The higher barrier of 3.4 kJ/mol found in the hindered environment of the solid ensures more limited vibrational motion near 0 K and hence a higher muon Hfcc. Assuming the same 0 K intercept for the muon Hfcc in the solid and (extrapolated) liquid-phase data is tantamount to assuming the same potential minimum in both phases, with the different T-dependences exhibited then being solely due to differing distributions of torsional states in the solid and liquid phases, as reflected in the differing barrier heights seen. We were also able to get an equally good fit to these data, including the liquid-phase data from ref 22, with the model of eq 10 on the basis of this same assumption, as shown by the fitted rust trend line in Figure 7 and giving a fitted barrier of 2.3 kJ/mol, entirely in accord with that reported in ref 7.

The very similar results found from fits to the data for Mu−*tert*-butyl, on the basis of the same assumption in both the solid and liquid phases here and in ref 7, helps to "benchmark" both the methodology and the calculated muon Hfcc from paper I employed herein.

Another point of view though, anticipated by the discontinuity seen in $A'_\mu(T)$ at the phase transition in Figure 7, is that environmental effects influence not only the distribution of torsional states (and hence barrier heights) but also the spin density itself at the potential minimum, thereby directly enhancing the muon Hfcc in the solid phase. Support for this view is found from the MP2-calculated value of 131 MHz for $A'_\mu(0)$ from paper I (unfilled green circle), which is much lower than both the measured value and the B3LYP-calculated value of 154 MHz at 0 K given above. These MP2-calculated Hfcc also give an equally good fit of eq 10 to the liquid-phase data for muoniated *tert*-butyl, shown by the green trend line, as that found from the B3LYP calculations on the basis of the assumption of phase-independent muon Hfcc at 0 K discussed above (rust trend line). The MP2 fit gives a modestly higher fitted barrier of 3.9 kJ/mol, necessiated by the lower intercept and flatter T-dependence of the $A'_\mu(T)$ data in the liquid phase.

Our intrepretation of this result is that the MP2 calculations intrinsically give a much better account of the $A'_\mu(T)$ data in the *absence* of lattice interaction effects, consistent with the comparisons carried out in paper I for the muoniated ethyl radical, and where, significantly, there is no discontinuity in $A'_\mu(T)$ at the phase transition (see ref 11). This comparison in turn suggests that the DFT/B3LYP calculations of muon Hfcc, despite the excellent fit to the *tert*-butyl data seen in Figure 7, tend to fortuitously mimic environmental effects that enhance the muon Hfcc in the solid phase, probably due to error cancellations in the method. Even so, both the large Hfcc seen near 0 K and the discontinuity in $A'_\mu(T)$ could still be partly due to the aforementioned effect of hindered vibrational motion in the solid phase, which could then suddenly "relax" at the phase transition. Results very similar to those discussed above for muoniated *tert*-butyl are found for the *trans-sec*-butyl radical below (Figure 6), but not for the *sec*-butyl radical formed from 1-butene (Figure 3), discussed next.

5.2. *sec*-Butyl (and *n*-Butyl) Radicals from 1-Butene. *5.2.1. Muon Hfcc,* $\boldsymbol{A'_\mu(T)}$. The structural formula of the *sec*-butyl radical formed from Mu addition to 1-butene is $CH_3CH_2\dot{C}HCH_2$ Mu. As discussed in paper I, the most stable conformer of 1-butene is its gauche form and from Mu addition the most stable *sec*-butyl radical expected to form is the s1 (trans) conformer. Since the muon is placed in the terminal methyl group, as in muoniated *tert*-butyl, its muon Hfcc, $A'_\mu(T)$, might be expected to exhibit behavior similar to that seen in Figure 7.

However, in contrast to Mu−*tert*-butyl, the muon Hfcc for the Mu−*sec*-butyl radical plotted in Figure 3 (blue data points) show no obvious sign of any discontinuity in $A'_\mu(T)$ at the bulk melting point of 1-butene (88 K, vertical dashed line), though, as remarked before, a small gap cannot be ruled out. An acceptably good fit of eq 10 to the continuous temperature dependence seen for the $A'_\mu(T)$ data is found, assuming muon Hfcc from the s1 conformer, as shown by the blue fitted line. However, and also in contrast to Mu−*tert*-butyl, the fit here is from the MP2-calculated muon Hfcc, though giving a torsional barrier that is essentially the same, V_2 = 2.9 kJ/mol. Both the $A'_\mu(0)$ value of 139.5 MHz (open blue triangle) and the fitted trend for $A'_\mu(T)$ from these MP2 calculations are in good overall agreement with the data in both the solid and liquid phases, falling just below the experimental trend at the lowest temperatures and just above near the phase transition. This degree of scatter may be partly due to the fact that the Mu−*sec*-butyl radical does not have the same C_s symmetry as Mu−*tert*-butyl, so the calculated muon Hfcc are no longer symmetric

about the potential minimum near ±120° (Table 1, paper I), as assumed in the torsional potential of eq 7. The B3YLP result for the s1 conformer at 0 K is 157 MHz (not plotted), well above experiment and the fit to the $A'_\mu(T)$ data from these calculated muon Hfcc is correspondingly worse. It can also be noted that the MP2-calculated value for the s3 (cis) conformer from paper I is 122 MHz at 0 K, far too low to account for the data.

The fact that there is no real gap seen in $A'_\mu(T)$ for the *sec*-butyl radical at the melting point of 1-butene suggests that environmental effects on muon Hfcc in the solid phase play only a minimal role here, in contrast to the Mu−*tert*-butyl case commented on above. This is in accord as well with the relatively good fit obtained from the MP2-calculated muon Hfcc, consistent with the fit to the liquid-phase data for muoniated *tert*-butyl in Figure 7, and with the view expressed in paper I that the MP2 theory intrinsically gives much better agreement with measured muon Hfcc in the absence of environmental effects.

The Hfcc data for $A'_\mu(T)$ shown by the black inverted-triangle data points in Figure 3 could arise from a number of possible conformers of the *n*-butyl or *sec*-butyl radicals, all with similar calculated Hfcc (paper I) and with only three values (in the liquid phase) it is not possible to reliably distinguish between these different posibilites. The calculated value of 143.5 MHz shown by the unfilled inverted triangle at 0 K and the black trend line shown, a fit of eq 10 to the data, assumes the formation of the most stable (n3) conformer of the primary *n*-butyl radical, with the structural formula $CH_3CH_2CHMu\dot{C}H_2$, formed by Mu addition to the gauche form of 1-butene, and is also from the MP2-calculated muon Hfcc of paper I. This gives a better fit than assuming the formation of less stable *sec*-butyl conformers and supports a tentative conclusion of having observed the muoniated *n*-butyl radical here. The torsional barrier from the fit is $V_2 = 3.9 \pm 0.3$ kJ/mol, though not overly reliable, considering that it is based on only three data points. It is noteworthy though that theory does reflect the experimental result of a higher muon Hfcc for what is assumed to be the primary *n*-butyl radical compared to *sec*-butyl.

5.2.2. Proton Hfcc, $A_{p,CH_2}(T)$ and $A_{p,CH_2Mu}(T)$. The experimental *T*-dependence of the methylene proton Hfcc for muoniated *sec*-butyl, $A_{p,CH_2}(T)$, shown by the red diamonds in Figure 3, is significant in two respects. First, the value of these Hfcc at 0 K is large, about 125 MHz (extrapolated), which can only be due to an *eclipsed* C−H bond of the $-CH_2$ methylene group, in like manner to that seen for C−Mu from $-CH_2Mu$. Second, there is a clear, albeit small, discontinuity in the data at the bulk melting point (88 K), again suggestive of environmental effects affecting Hfcc in the solid phase, but here, and also for the terminal methyl group of the *trans*-2-butyl radical below (Figure 6), for *proton* Hfcc.

Recognzing the few percent level of scatter that could be expected from either the data or from the fit to $A'_\mu(T)$ above, our first attempt was to fit these $A_{p,CH_2}(T)$ results to a single line from the model of eq 10. However, while the B3LYP calculations (s1 conformer) give a good account of the data in the solid phase (fitted red line), including the 0 K value of 124 MHz (unfilled red diamond), the high-temperature free rotation limit from these calculations is 85.2 MHz, far too high to account for the asymptotic trend from the liquid-phase data. A similar attempt using MP2-calculated proton Hfcc for s1 had the opposite problem, with the calculated high-temperature limit of 69.2 MHz in good agreement with this trend, as shown by the fitted orange line, but with the calculated value at 0 K of 113 MHz (open orange circle) falling well below experiment in the solid phase.

This seeming disconnect might be partly due to the aforementioned point that the calculated Hfcc are not symmetric about 120°, as assumed from eq 7, or it may also indicate a more complex situation involving a mixture of three different posible *sec*-butyl conformers in the liquid phase from the calculations of paper I: *trans*-butyl (s1), *cis*-butyl (s3), and a conformer of intermediate geometry (s2). The most likely contribution here would be from the s3 conformer, with an MP2-calculated value of 110 MHz at 0 K, very similar to the s1 result. The s2 conformer does not have an eclipsed C−H bond and thus does not contribute in the solid phase, but the higher temperatures of the liquid might facilitate intercoversion between all three, possibly contributing then to a reduced averaged Hfcc in the liquid phase and hence to the discontunity seen in $A_{p,CH_2}(T)$ as well.

However, both the similarity in MP2-calculated values at 0 K for the trans and cis conformers and the good quality of the separate fits seen in Figure 3 on the basis of assuming just the trans conformer, supports the claim herein that even the small gap in $A_{p,CH_2}(T)$ at the 1-butene melting point is largely due to environmental effects. This situation is reminicent of that for $A'_\mu(T)$ from fitting the data for the muoniated *tert*-butyl radical in Figure 7, and the model fits for $A_{p,CH_2}(T)$ in Figure 3 can be interpreted in the same way: namely the B3LYP calculations (fitted red trend line) again mimic the effect of lattice interactions in the solid which are otherwise better predicted by the MP2 calculations in the absence of these interactions (orange trend line). The fitted torsional barriers are very similar in both cases, $V_2 = 1.4$ kJ/mol in the solid and 1.5 kJ/mol in the liquid phase. It is noteworthy that the two EPR data points for the methylene protons, shown by the black crosses in the figure, fall exactly on the fitted (orange) trend line in the liquid phase. In this case little or no isotopic effect would be expected, as observed.

There is another possible contributing mechanism here though, which also resonates with the *trans*-2-butyl case discussed below. The methylene protons in the *sec*-butyl radical are in the ethyl group adjacent to the radical center, and since the nearby bulky γ-methyl can be expected to have a preference to lie in the nodal plane at low temperatures, ethyl rotation about the $C_\alpha-C_\beta$ bond with increasing temperature causes more repulsion between the terminal CH_3 and CH_2Mu groups, perhaps coupled to some torsional distortion of the carbon skeleton as well, possibly contributing then to the small gap seen in $A_{p,CH_2}(T)$ at the melting point. Such a torsional distortion effect would be expected to have a lesser impact on the $-CH_2Mu$ group, which, though also adjacent to the radical center, is at the end of the molecule and so has more freedom of movement, consistent with little or no gap seen in $A'_\mu(T)$ at the melting point in Figure 3.

The second set of proton Hfcc, for the *staggered* protons of the $-CH_2Mu$ group of the *sec*-butyl radical, $A_{p,CH_2Mu}(T)$, are shown by the magenta squares and fitted trend line in Figure 3 and are largely the mirror image of the $A'_\mu(T)$ dependence, as would be expected. Though, as above, these proton Hfcc (near ±120°) are quite nonsymmetric, assuming to first order that the average that would be observed (no additional Δ_0 resonance is seen) gives a Hfcc of 37.5 MHz from the B3LYP calculations of paper I, shown by the open square plotted in Figure 3, with the magenta trend line the fit of eq 11 to the *T*-dependence of the data from these B3LYP-calculated Hfcc. The overall quality of the fit is good to excellent and gives a fitted torsional barrier of $V_2 = 2.2$ kJ/mol, somewhat lower than the 2.9 kJ/mol value found from fitting the $A'_\mu(T)$ data, indicative of non-rigid-rotor bond rotation for $-CH_2Mu$. (Fitting both data sets simultaneously, as eq 7 would imply, produced a worse fit to particularly these $-CH_2Mu$ proton Hfcc.)

It is noteworthy that there is no discontinuity in the proton Hfcc for $A_{p,CH_2Mu}(T)$ at the melting point of 1-butene in Figure 3, in contrast to that for the eclipsed $-CH_2$ protons discussed above. This supports the general theme advanced in paper I, from comparisons with muoniated ethyl, where there is also no discontinuity at the bulk melting point (ref 11), that the B3LYP calculations consistently give the best agreement between theory and experiment for the staggered proton Hfcc of Mu-substituted alkyl groups. For comparison, the MP2 calculation of paper I gives an average Hfcc of 28 MHz at 0 K here, for the s1 conformer, with high temperature values that are also too low to agree with the trend in the $A_{p,CH_2Mu}(T)$ data.

The high-temperature free rotation limit of the B3LYP calculations for $-CH_2Mu$ from paper I is 77 MHz, similar to but somewhat higher than that for the methyl proton Hfcc from EPR measurements for the unsubstituted *sec*-butyl radical,[1,2,4] shown by the solid green circles and the dashed black line in Figure 3 that gives the B3YLP free rotation limit of 72 MHz. This difference indicates a small "residual isotope effect" similar to that reported for $-CH_2Mu$ of the Mu−*tert*-butyl radical in Ref 7. The EPR data have only been measured over the temperature range 175−298 K and are consistent with a low torsional barrier of ∼100 J/mol, which would be in marked contrast with early ab initio calculations of Carmichael that predict a barrier for methyl rotation in the *sec*-butyl radical of ∼2 kJ/mol.[40]

The third set of proton Hfcc seen are plotted as the black asterisks in Figure 3 (bottom). The relatively low Hfcc values as well as the weak intensities seen follow directly from the high-field positions of their assumed Δ_0 resonances (Figure 2, bottom scan). With only three, relatively closely spaced values, the origin of these proton Hfcc cannot be identified. The best agreement with theory is found by assuming that they are due to the protons of the $-CH_2Mu$ group of the s3 (cis) *sec*-butyl conformer, but other possibilities such as the single proton of −CHMu for the primary *n*-butyl radical cannot be excluded.

5.3. *sec*-Butyl Radicals from *cis*- and *trans*-2-Butene. The *T*-dependences of the muon Hfcc, $A'_\mu(T)$, for the −CHMu group of the *sec*-butyl radicals formed from Mu addition to *cis*- and *trans*-2-butene, along with the measured proton Hfcc, $A_{p,CH_3}(T)$ and $A_{p,CHMu}(T)$, from the entries in Table 2, are plotted in Figure 6. Only one muoniated radical is formed in each case, with the structural formula $CH_3\dot{C}HCH\ MuCH_3$, but giving separate *cis*- and *trans*-butyl conformers in the solid phase. For the unsubstituted *sec*-butyl radical, this is the same environment whether formed (by H-atom addition) to 1-butene or 2-butene, but not so for the muoniated radicals.

5.3.1. Muon Hfcc, $A'_\mu(T)$. The muon Hfcc again exhibit clear (McConnell) plateaus near 0 K in Figure 6 for both the *cis*- and *trans*-2-butyl radicals, with a small but distinct difference seen in $A'_\mu(T)$ for the cis isomer (solid inverted black triangles and *guideline* to the eye), about 6 MHz above the trans (blue points and fitted trend line), indicating the preservation of the geometry of the 2-butene parent isomers in the solid phase. In contrast, the muon Hfcc are essentially identical in the liquid phase (Table 2), demonstrating facile interconversion and equal molecular interactions betweeen the *cis*- and *trans-sec*-butyl conformers at the higher temperatures.

Like the muoniated *tert*-butyl radical (Figure 7), but in contrast to Mu−*sec*-butyl formed from 1-butene discussed above (Figure 3), there is a sharp discontinuity in $A'_\mu(T)$ at phase transitions here and, distinctively, precisely at the separate melting points of each parent geometrical isomer, 134 K for cis (vertical dashed line) and 168 K for trans (vertical dotted line), demonstrating the sensitivity of the μSR technique to subtly changing molecular environments. This observation of a gap in $A'_\mu(T)$ at the *sec*-butyl melting points also demonstrates lattice interactions and hindered rotation in the solid phase, in like manner to that commented on earlier for Mu−*tert*-butyl.

The B3LYP calculation of paper I gives 145 MHz for $A'_\mu(0)$ for the *trans*-2-butyl radical (unfilled blue triangle in Figure 6), a few megahertz above but otherwise in seeming good agreement with the extrapolated experimental value of about 140 MHz. (No energy minimum could be found for the cis isomer from the B3LYP calculation.) The broad plateau and shallow slope of $A'_\mu(T)$ for the trans radical is also well represented by the blue fitted line to eq 10 shown, determined from these B3LYP-calculated muon Hfcc, and giving a torsional barrier of $V_2 = 3.0 \pm 0.2$ kJ/mol in the solid phase, very similar to that found for Mu−*tert*-butyl in Figure 7 and also to that from the MP2-calculations for *sec*-butyl from 1-butene (Figure 3). As with the 0 K intercept, the fitted trend for the *trans*-butyl radical is a few megahertz above the measured muon Hfcc at the lower temperatures but is otherwise in good agreement with the overall temperature dependence up to the melting point. The similarities in fitted torsional barriers found for C−Mu bond rotation in different muoniated butyl radicals, independent of calculational detail, suggests that these are mainly determined by ZPE rather than by environmental effects.

In parallel with the "benchmark" results discussed above for Mu−*tert*-butyl, a fit of the $A'_\mu(T)$ data for the *trans*-2-butyl radical to the model of eq 10, assuming the same 0 K value for $A'_\mu(0)$ in the liquid as in the solid phase, was expected to give an equally satisfactory "fit" to the liquid-phase data. However, such is not the case, as shown by the very poor fit to the data represented by the rust-brown trend line for the B3LYP-calculated muon Hfcc in Figure 6. The much better agreement noted earlier for muoniated *tert*-butyl on the basis of this assumption (Figure 7), which may be partly due to the more symmetric nature of the *tert*-butyl radical commented on earlier, supports the suggestion made herein that it is more than just an effect due to the distribution of torsional states and hindered rotation in the solid, seen in the change in torsional barriers, that is responsible for the differing temperature dependences for $A'_\mu(T)$ in the solid and liquid phases. Rather, the enhanced muon Hfcc seen in the solid, and hence the gap at the phase transition, may be the result of intrinsically enhanced spin densities arising from specific intermolecular interactions between the radical and its host environment at low temperatures, a feature that appears to be common to both the muoniated *tert*-butyl (Figure 7) and *trans*- and *cis*-2-butyl radicals (Figure 6) but, interestingly, is not observed for the *sec*-butyl radical from 1-butene (Figure 3). This dichotomy may be related to the more single-crystal-like nature of the planar isobutene and 2-butene precursors in contrast to the more polycrystalline nature of 1-butene, noted previously (see also paper I).

Thus, as for the *tert*-butyl case (Figure 7), the seeming good agreement seen between the B3LYP theory and experiment for $A'_\mu(T)$ for *trans*-2-butyl in the solid phase (Figure 6) is likely also more fortuitous than real, again probably the result of error cancellations in the DFT/B3LYP method that artificially mimic the effect of lattice interactions enhancing the muon Hfcc. In concert with this view, the MP2-calculated value for $A'_\mu(0)$ of 127 MHz (unfilled green circle) falls well below the experimental intercept of 140 MHz, with a similar difference for the *cis*-butyl radical, giving 124 MHz at 0 K (not plotted). The green trend line shown in Figure 6 is a fit of all the $A'_\mu(T)$ data in the liquid phase, extrapolated to 0 K, to the model of eq 10, assuming the MP2-

calculated muon Hfcc for the s1 (trans) conformer of paper I. The good fit seen gives a reasonable torsional barrier of V_2 = 3.7 kJ/mol but is in marked contrast to the very poor fit shown to the liquid-phase data from the B3LYP calculations on the assumption of phase-independent muon Hfcc at 0 K (rust-brown line).

However, there is an important distinction here compared to the muoniated *tert*-butyl radical. There is only one *tert*-butyl conformer, but as noted earlier from 1-butene, there are *three* possible *sec*-butyl conformers: s1 (trans), s3 (cis), and s2 (of intermeadiate geometry). In contrast to *sec*-butyl from 1-butene though, where there is some uncertainty in which conformer is being formed (though s1 gives the best result for $A'_\mu(T)$ near 0 K), a much clearer case is presented by Mu addition to *cis*- and *trans*-2-butene, where the geometries of the parent isomers are preserved in the solid phase (Figure 6). The MP2 fit shown to the trans liquid-phase data for the muon Hfcc (green line) assumes formation of the s1 (trans) conformer only, but if the s3 (cis) conformer is assumed, with its slightly lower $A'_\mu(0)$ intercept of 124 MHz, the fit is almost the same (not shown). Thus we conclude that the very poor quality of the B3LYP fit to the liquid-phase data, assuming that the 0 K muon Hfcc is phase-independent (rust line) is little influenced by cis−trans interconversion in the liquid phase, supporting the claim herein that the values for $A'_\mu(0)$ are indeed phase-dependent.

That having been said, the effect of a change in the occupancy of various torsional or vibrational states at the phase transition, as proposed in ref 7, is likely contributing in a synergistic fashion as well, depending both on the nature of the precursor alkene and on the muoniated radical that is formed. In this regard a further caveat is introduced in the present case by the unknown role played by the s2 conformer on the muon Hfcc of the *sec*-butyl radical. Though this is not formed in the solid phase from 2-butene (though it is from 1-butene, paper I), interconversion between all three conformers is possible at the higher temperatures of the liquid phase. As previously commented on, this could give rise to a reduced thermal-averaged Hfcc in the liquid, thereby contributing to the gap seen for $A'_\mu(T)$ in Figure 6, as suggested earlier in the case for $A_{p,CH_2}(T)$ from 1-butene (Figure 3). However, such an effect is unlikley to be dramatic enough to account for more than a small part of the large gap seen for $A'_\mu(T)$ in Figure 6.

5.3.2. Proton Hfcc, $A_{p,CH_3}(T)$ and $A_{p,CHMu}(T)$. The data set for the proton Hfcc of the terminal CH_3 group, $A_{p,CH_3}(T)$, shown by the red diamonds and fitted red line of eq 10 to the data in the solid phase in Figure 6, is significant in several respects. First, it is another example of large proton Hfcc seen near 0 K, due to eclipsed C−H bonds, as in the case for the methylene protons from 1-butene (Figure 3), but here due to the terminal methyl protons.

Second, both the calculated 0 K value of 124 MHz shown by the open red diamond in Figure 6 and the fitted trend line to eq 10 are in good, if not very good, agreement with experiment but are from the *MP2-calculated* proton Hfcc of paper I. This appears to be in conflict with expectations from the ("benchmark") calculations carried out for muoniated ethyl in paper I, which suggest that better agreement with experiment is to be expected from the B3LYP-calculated proton Hfcc. However, the B3LYP calculation for $A_{p,CH_3}(T)$ here gives 135 MHz for *trans*-2-butyl at 0 K, well above experiment and correspondingly gives a worse fit to the T-dependence as well. It is important to realize, though, that these MP2 calculations of proton Hfcc are for *eclipsed* methyl protons in contrast to the staggered protons of $-CH_2Mu$ in the case of the muoniated ethyl radical. The fitted barrier from the MP2-calculated proton Hfcc is V_2 = 4.7 ± 0.3 kJ/mol, a relatively high value compared to the lower barrier found for *sec*-butyl in Figure 3, but consistent with the extended McConnell plateau region and flat T-dependence seen for these proton Hfcc at the lower temperatures in Figure 6.

The third and most unexpected feature of these data is the remarkable discontinuity seen in $A_{p,CH_3}(T)$ at the melting point of *trans*-2-butene, 168 K (vertical dotted line), which can be contrasted with the modest gap seen in the case of the methylene protons ($-CH_2$) of the *sec*-butyl from 1-butene (Figure 3). A literature search reveals no previous mention of such discontinuities in proton Hfcc, nor of their aforementioned large values near 0 K, from either μSR or EPR studies of alkyl radicals. Since a similar, albeit less dramatic, discontinuity is seen for $A'_\mu(T)$ in the *trans*-2-butyl radical here (Figure 6), as well as for the *tert*-butyl radical (Figure 7), these data collectively demonstrate that environmental effects can alter the spin densities of *both* muon and proton Hfcc in the solid phase.

The small torsional barrier of ∼100 J/mol indicated for the proton Hfcc of *un*substituted methyl groups, commented on earlier (from Figure 3), raises the question of why such a large barrier height is seen for the terminal methyl group of the muoniated *trans*-2-butyl radical here (also indicated for the cis radical, but with insufficient data to be established), as well as how this is accociated with the dramatic discontinuity seen in $A_{p,CH_3}(T)$ at the neat melting point.

A clue to the origin of both of these effects is provided by the fact that the C−Mu bond of the trans (and cis) radical from 2-butene is at the methylene position, adjacent to the radical center, in like manner to that for the $-CH_2$ group of the *sec*-butyl radical formed from 1-butene (the fitted red trend line in Figure 3). Similar to that case, the rotating ethyl group containing the C−Mu bond, with its naturally high barrier, may cause additional steric repulsion here between terminal methyl groups, thereby quite likely also directly enhancing the barrier to β-CH_3 rotation, and which again could be interactive with additional distortion of the backbone carbon chain. This suggestion receives support from noting that the barrier heights and T-dependences for $A'_\mu(T)$ and $A_{p,CH_3}(T)$ are quite similar in the solid phase (Figure 6). However, the degree to which such torsional interaction effects are important (or not) for muoniated *sec*-butyl radicals can only be established by high level ab initio calculations that include both intramolecular and host−guest interactions, an approach that goes well beyond the calculations carried out in paper I.

Another observation is worthy of a brief comment here. The data for $A_{p,CH_3}(T)$ *above* the melting point, shown by the red diamond data points and short broken red guide line in Figure 6, appear to merge with the proton Hfcc for −CHMu, as drawn, consistent with the ALC spectra shown in Figure 5. However, these values could almost be T-independent, with essentially the same average Hfcc for the free rotor limit (72 MHz) as plotted in Figure 3 for the *un*substituted *sec*-butyl radical (solid green data points and dashed black line), as would be expected for the same environment.

The magenta trend line shown at the bottom of Figure 6 is a model fit of eq 11 to the data (magenta squares) for the (single) *staggered* proton of the Mu-substituted methylene group, −CHMu of the *trans*-2-butyl radical, $A_{p,CHMu}(T)$, and harking back to the remarks above, *is* from the B3LYP-calculated proton Hfcc of paper I. The data for the cis radical (solid green circles) are very similar, in both the solid and liquid phases (see also Table 2), but are not included in the fit. (As mentioned, there was no B3LYP minimum found for the cis conformer.) The B3LYP-calculated proton Hfcc at 0 K is 64 MHz, shown by the open magenta square in the figure, is in excellent agreement with the trend in the data, as is the fitted line itself, giving a barrier of V_2 = 5.6 ± 0.4 kJ/mol. The MP2 calculation

for −CHMu gives 37 MHz at 0 K here, almost a factor of 2 lower than the experimental intercept. The magnitude of the fitted barrier for C−H bond rotation here contrasts sharply with the 3.0 kJ/mol value found above for C−Mu and again indicates non-rigid-rotor internal rotation of Mu-substituted alkyl groups.

As in the case for muoniated ethyl (see ref 11), there is no discontinuity in the staggered proton Hfcc for these muoniated *sec*-butyl radicals at bulk melting points, for $A_{p,CHMu}(T)$ here and earlier for $A_{p,CH_2Mu}(T)$ for the *sec*-butyl radical from 1-butene (Figure 3). It remains unclear though why the $A'_\mu(T)$ data for these same Mu-substituted alkyl groups do show marked discontinuities at melting points for the *cis*- and *trans*-2-butyl radicals formed from 2-butene (Figure 6) but not for the *sec*-butyl radical formed from 1-butene (Figure 3). This may be due to the location of the C−Mu bond, as commented on earlier. However, there is also an important point from paper I that deserves mention here. The DFT/B3LYP method was developed in part to account for EPR-measured proton Hfcc and so the efficacy of this method could well be less in the case of isotopomers and in particular for muoniated radicals.

6. SUMMARY AND CONCLUDING REMARKS

Reported in this paper is a first study of the muon and β-proton hyperfine coupling constants (Hfcc) for muoniated *sec*-butyl radicals, complementing earlier-reported work for the Mu−*tert*-butyl radical[7] (also shown in Figure 7). As in that study, the temperature dependences of the data for the muon Hfcc (Figures 3 and 6), exhibit clear "McConnell plateaus" at the lower temperature due to the eclipsed C−Mu bond at its energy minimum. Less well known, and to our knowledge not previously established for alkyl radicals, is that similar plateaus and large Hfcc near 0 K are also observed for proton Hfcc, due to eclipsed C−H bonds, here for the methylene and methyl proton Hfcc of the *sec*-butyl radicals studied.

The experimental data for the (reduced) muon, $A'_\mu(T)$, and β-proton, $A_p(T)$, Hfcc are compared with in vacuo MP2 and DFT/B3LYP calculations of Hfcc at 0 K reported in the previous paper (I), both with EPR-III basis sets. In most cases the agreement between theory and experiment for the measured Hfcc both near 0 K and in model fits to the temperature dependences for $A'_\mu(T)$ and $A_p(T)$ is almost quantitative, typically within 10% or better. However, there are several qualifications associated with this level of agreement that are related to environmental effects.

A simple model assuming the 2-fold torsional potential $V_2(\theta) = {}^1/_2V_2(1 - \cos 2\theta)$, in conjunction with a Boltzmann weighting of the calculated Hfcc at energy minima of 0 and near $\pm 120°$ from paper I, was employed to fit the data for both $A'_\mu(T)$ and $A_p(T)$, providing an assessment of the validity of the calculated Hfcc as well an estimate of torsional barriers, V_2, to internal rotation. Barriers to C−Mu bond rotation for Mu-substituted alkyl groups were found to be ∼3 kJ/mol for all muoniated butyl radicals, suggesting that ZPE effects play the dominant role in determining these barrier heights rather than differences in molecular geometry or environment. In contrast, for eclipsed C−H bonds, torsional barriers vary by an order of magnitude, depending on the nature of environmental effects.

Compared to Mu−*tert*-butyl, the muoniated *sec*-butyl radicals are much more complex systems than might have been expected at first glance, with markedly different results seen that are interpreted as being due to intra- and intermolecular (lattice) interactions. These environmental effects could also be related to different possible *sec*-butyl conformers formed and to the location of the C−Mu bond and perhaps as well on the solid-state structure of the parent 1-butene (more polycrystalline) and 2-butene (more crystalline) alkenes in the solid phase.

This complexity, revealing the subtlety of the molecular interactions involved, can be seen immediately in comparing the results for $A'_\mu(T)$ for the *sec*-butyl radicals formed. From 1-butene this temperature dependence exhibits no obvious gap at the bulk melting point (Figure 3), indicative of little or no environmental effect on the muon Hfcc in the solid phase, and accordingly both the value for $A'_\mu(0)$ and the trend with temperature seen for $A'_\mu(T)$ are well predicted by the MP2 level of theory for muon Hfcc, in accord with benchmark calculations carried out in paper I for the muoniated ethyl radical. In contrast, $A'_\mu(T)$ for the *trans*- and *cis*-2-butyl radicals, formed from their parent 2-butene geometric isomers, show clear discontinuities precisely at their respective bulk melting points, with the muon Hfcc abruptly enhanced in the solid, and where the B3LYP calculations for $A'_\mu(T)$ seemingly give much better agreement with experiment than MP2 (Figure 6). Similar results are seen for the muoniated *tert*-butyl radical (Figure 7).

There are two possible interpretations for this abrupt enhancement on the muon Hfcc here. One is that the distribution of torsional states is phase-dependent but with the values of $A'_\mu(0)$ being phase-independent, leading to different barriers from fits to $A'_\mu(T)$ in the solid and liquid phases, a view advanced in ref 7 for the muoniated *tert*-butyl radical. The same view has been explored here as well utilizing B3LYP-calculated muon Hfcc in both phases. However, it is felt that the good agreement found with experiment for $A'_\mu(T)$ is largely fortuitous, the result of the DFT/B3LYP calculations mimicking the effect of environment on the muon Hfcc in the solid phase. Alternatively, the muon Hfcc can be intrinsically phase-dependent, with the spin density at the muon ehanced due to molecular interactions in the solid phase. This is the view advanced herein and supported by the result that MP2-calculated muon Hfcc give the best agreement between theory and experiment in the *absence* of environmental effects. In reality, both contributions are likely acting synergistically, depending on the location of the C−Mu bond and on the solid-state structure of the parent butenes.

The impact of environmental effects and the complexity of molecular interactions is also seen in the proton Hfcc for the *sec*-butyl radicals in the present study. Four distinct proton environments have been identified and their Hfcc compared with theory: the eclipsed $-CH_2$ and staggered $-CH_2Mu$ protons of *sec*-butyl formed from 1-butene, and the eclipsed CH_3- and staggered −CHMu protons of *cis*- and *trans*-2-butyl formed from the 2-butenes. To our knowledge these are the most detailed studies to date of proton Hfcc for alkyl radicals. The C−H bonds of both eclipsed proton environments give large proton Hfcc near 0 K, in like manner to C−Mu, and similarly as well show clear McConnell plateaus. They also both exhibit clear discontinuities in $A_p(T)$ at bulk melting points.

In the case of the methylene protons from 1-butene (Figure 3), good agreement is found for $A_{p,CH_2}(T)$ from B3LYP-claculated proton Hfcc in the solid phase, but in the liquid phase better agreement is found from the MP2 calculations, behavior that is similar to $A'_\mu(T)$ for *trans*-2-butyl. In contrast, for the methyl protons of *sec*-butyl from 2-butene (Figure 6), which exhibit a truly dramatic discontinuity at the *trans*-2-butene melting point, the proton Hfcc $A_{p,CH_3}(T)$ in the solid phase are in much better agreement with the MP2 calculations. It is suggested that there is a cooperative effect on torsional C−Mu bond rotation at its methylene position adjacent to the radical center in the 2-butyl radicals, coupled with distortion of the backbone carbon skeleton, that brings the terminal γ- and

β-CH_3 groups into closer proximity, thereby facilitating methyl−methyl repulsion and giving rise to the relatively large fitted torsional barrier of 4.7 kJ/mol seen for the *trans*-2-butyl radical. This is also dictated by the large Hfcc and broad plateau region seen (Figure 6). A similar though less dramatic effect is seen for the central methylene protons of *sec*-butyl from 1-butene, giving rise to the much lower fitted torsional barrier of 1.5 kJ/mol.

In contrast to the T-dependence of the proton Hfcc for eclipsed protons, that for the *staggered* protons, $A_{p,CH_2Mu}(T)$ from 1-butene and $A_{p,CHMu}(T)$ from 2-butene, are more consistently predicted by theory, the B3LYP calculations providing good to excellent agreement with the trends seen in both cases, in accord with the benchmark calculations carried out in paper I for the muoniated ethyl radical. As would be expected, these are largely the mirror image dependences of those seen for the corresponding muon Hfcc, but with fitted torsional barriers that are not the same, lower for $A_{p,CH2Mu}(T)$ and higher for $A_{p,CHMu}(T)$, suggesting non-rigid-rotor internal rotation of the Mu-substituted alkyl groups. In contrast as well to the eclipsed protons, there are *no* discontinuites seen at neat melting points for either $A_{p,CH_2Mu}(T)$ or $A_{p,CHMu}(T)$, with essentially identical trends found for both cis and trans conformers in the latter case.

The continuous trend seen for the staggered $-CH_2Mu$ protons from 1-butene is in accord with the trend seen for $A'_\mu(T)$ in that case, but not for the $-CHMu$ proton from 2-butene, where $A'_\mu(T)$ exhibits a clear discontinuity. It is suggested that this difference is related to the location of the C−Mu bond in these different *sec*-butyl radicals: at the end of the molecule from 1-butene, where it has more freedom of movement, but at the central methylene position from 2-butene, where concerted C−Mu bond rotation and backbone carbon torsional motion contributes also to the unusually high barrier for C−H bond rotation of 5.6 kJ/mol.

The present results for muoniated *sec*-butyl radicals represent an important extension of comparisons between theory and experiment for alkyl radicals beyond the simplest and well-studied ethyl radical. These *sec*-butyl reaction systems are complex, as shown by the markedly different behavior seen for the T-dependences of both their muon and proton Hfcc, which reflect the subtle nature of molecular interactions revealed by these μSR studies, effects that go well beyond the in vacuo DFT/B3LYP and MP2 calculations of paper I compared with herein. Even so, overall, these single-molecule calculations perform surprisingly well.

AUTHOR INFORMATION

Corresponding Author

*E-mail: flem@triumf.ca.

Present Addresses

[†]Department of Chemistry and Biochemistry, and the Jules Stein Eye Institute, UCLA, Los Angeles, CA, 90095−1569.

ACKNOWLEDGMENT

We thank Dr. Syd Kreitzman and the technical support staff of the Center for Molecular and Materials Sciences at TRIUMF and Dr. Khashayar Ghandi for his participation in the early stages of these experiments. Special thanks to Prof. Ian Carmichael of Notre Dame University for allowing us to refer to his unpublished calculations (ref 40). The Natural Sciences and Engineering Research Council of Canada (NSERC) is gratefully acknowledged for their financial support.

REFERENCES

(1) Fessenden, R. W.; Schuler, R. H. Electron Spin Resonance Studies of Transient Alkyl Radicals. *J. Chem. Phys.* **1963**, *39*, 2147–2195. Fessenden, R. ESR Studies of Internal Rotation in Radicals. *J. Chim. Phys. Phys.—Chim. Biol.* **1964**, *61*, 1570–1575.

(2) Fischer, H. Electron Spin Resonance of Transient Alkyl Radicals during Alkyllithium-Alkyl Halide Reactions. *J. Phys. Chem.* **1969**, *73*, 3834–3838.

(3) Krusic, P. J.; Jesson, J. P.; Meakin, P. Electron Spin Resonance Studies of Conformations and Hindered Internal Rotation in Transient Free Radicals. *J. Phys. Chem.* **1971**, *75*, 3438–3453.

(4) Paul, H.; Fischer, H. Electron-Spin Resonance of Free-Radicals in Photochemical Reactions of Ketones in Solution. *Helv. Chim. Acta* **1973**, *56*, 1575–1594.

(5) Atherton, N. M. *Principles of Electron Spin Resonance*; Ellis Horwood: London, 1993.

(6) Roduner, E.; Percival, P. W.; Fleming, D. G.; Hochmann, J.; Fischer, H. Muonium-Substituted Transient Radicals Observed by Muon Spin Rotation. *Chem. Phys. Lett.* **1978**, *57*, 37–40.

(7) Percival, P. W.; Brodovitch, J. C.; Leung, S. K.; Yu, D.; Kiefl, R. F.; Luke, G. M.; Venkateswaran, K.; Cox, S. F. J. Intramolecular Motion in the Tert-Butyl Radical as Studied by Muon Spin Rotation and Level-Crossing Spectroscopy. *Chem. Phys.* **1988**, *127*, 137–147.

(8) Roduner, E. Polarized Positive Muons Probing Free-Radicals - a Variant of Magnetic-Resonance. *Chem. Soc. Rev.* **1993**, *22*, 337–346.

(9) Fleming, D. G.; Pan, J. J.; Senba, M.; Arseneau, D. J.; Kiefl, R. F.; Shelley, M. Y.; Cox, S. F. J.; Percival, P. W.; Brodovitch, J. C. Spin relaxation of muonium-substituted ethyl radicals ($MuCH_2CH_2\cdot$) in the gas phase. *J. Chem. Phys.* **1996**, *105*, 7517–7535.

(10) Martyniak, A.; Dilger, H.; Scheuermann, R.; Tucker, I. M.; McKenzie, I.; Vujosevic, D.; Roduner, E. Using spin polarised positive muons for studying guest molecule partitioning in soft matter structures. *Phys. Chem. Chem. Phys.* **2006**, *8*, 4723–4740.

(11) Bridges, M. D.; Arseneau, D. J.; Fleming, D. G.; Ghandi, K. Hyperfine interactions and molecular motion of the Mu-ethyl radical in faujasites: NaY, HY, and USY. *J. Phys. Chem. C* **2007**, *111*, 9779–9793. Bridges, M. D. *M.Sc. Thesis*, University of British Columbia, Vancouver, Canada, 2004.

(12) Ramos, M. J.; Mckenna, D.; Webster, B. C.; Roduner, E. Muon Spin Rotation Spectra for Muonium Isotopically Substituted Ethyl Radicals. *J. Chem. Soc., Faraday Trans. I* **1984**, *80*, 255–265. Ramos, M. J.; Mckenna, D.; Webster, B. C.; Roduner, E. Muon Spin Rotation Spectra for Muonium Isotopically Substituted Ethyl Radicals. *J. Chem. Soc., Faraday Trans. I* **1984**, *80*, 267–275.

(13) Roduner, E. Muon spin resonance - A variant of magnetic resonance. *Appl. Magn. Reson.* **1997**, *13*, 1–14.

(14) Cormier, P; Arseneau, D. J.; Brodovitch, J. C.; Lanzon, J. M.; Taylor, B. A.; Ghandi, K. Free Radical Formation in Supercritical CO2, Using Muonium as a Probe and Implication for H Atom Reaction with Ethene. *J. Phys. Chem. A* **2008**, *112*, 4593.

(15) Toriyama, K.; Iwasaki, M.; Nunome, K.; Muto, H. *J. Chem. Phys.* **1981**, *75*, 1633.

(16) Claxton, T. A.; Graham, A. M. A Chemical Interpretation of Vibrationally Induced Barriers to Hindered Internal-Rotation. *J. Chem. Soc., Faraday Trans. II* **1987**, *83*, 2307–2317.

(17) Suter, H. U.; Ha, T. K. A Theoretical-Study on the Internal-Rotation and Hyperfine Structures of the Ethyl Radical (CH3-CH2). *Chem. Phys.* **1991**, *154*, 227–236.

(18) Claxton, T. A.; Graham, A. M. An *Ab initio* Study of Propyl Radicals. *J. Chem. Soc., Faraday Trans. II* **1988**, *84*, 121–134.

(19) Webster, B.; Buttar, D. Vibrational behaviour of the carbon-muonium bond in the muonated ethyl radical. *J. Chem. Soc., Faraday Trans.* **1996**, *92*, 2331–2334.

(20) McKenzie, I.; Brodovitch, J-C.; Ghandi, K.; McCollum, B. M.; Percival, P. W. Hyperfine Coupling in Methyl Radical Isotopomers. *J. Phys. Chem. A* **2007**, *111*, 10625–10634.

(21) Pacansky, J.; Yoshimine, M. Theoretical-Studies on the Barriers for Internal-Rotation of the Methyl-Groups in the Tert-Butyl Radical. *J. Phys. Chem.* **1986**, *90*, 1980–1983. Yoshimine, M.; Pacansky, J. Theoretical-Studies on the Structure of Isobutane and the Tertiary-Butyl Radical. *J. Chem. Phys.* **1981**, *74*, 5168–5173.

(22) Roduner, E.; Strub, W.; Burkhard, P.; Hochmann, J.; Percival, P. W.; Fischer, H.; Ramos, M.; Webster, B. C. Muonium Substituted Organic Free-Radicals in Liquids - Muon Electron Hyperfine Coupling-Constants of Alkyl and Allyl Radicals. *Chem. Phys.* **1982**, *67*, 275–285.

(23) Chipman, D. M. Theoretical-Study of Hyperfine Coupling-Constants in Ethyl Radical. *J. Chem. Phys.* **1991**, *94*, 6632–6637.

(24) Carmichael, I. Ab initio Quadratic Configuration-Interaction Calculation of the Isotropic Hyperfine Coupling-Constants in the Ethyl Radical. *J. Phys. Chem.* **1991**, *95*, 6198–6201.

(25) Bohm, M. C.; Ramirez, R.; Schulte, J. Finite-temperature properties of the muonium substituted ethyl radical CH(2)MuCH(2): nuclear degrees of freedom and hyperfine splitting constants. *Mol. Phys.* **2005**, *103*, 2407–2436.

(26) Ghandi, K.; Zahariev, F. E.; Wang, Y. A. Theoretical studies of alkyl radicals in the NaY and HY zeolites. *J. Phys. Chem. A* **2005**, *109*, 7242–7250.

(27) Senba, M.; Fleming, D. G.; Arseneau, D. J.; Garner, D. M.; Reid, I. D. Muonium Depolarization by Electron-Spin Exchange with O-2 Gas in the Temperature-Range 90−500-K. *Phys. Rev. A* **1989**, *39*, 3871–3883.

(28) Kreitzman, S. R.; Roduner, E. Theory of Avoided Level-Crossing Relaxation Dynamics for Axial Muonated Radicals. *Chem. Phys.* **1995**, *192*, 189–230.

(29) Duchovic, R. J.; Wagner, A. F.; Turner, R. E.; Garner, D. M.; Fleming, D. G. The Analysis of Muonium Hyperfine Interaction Measurements of Thermal Rate Constants for Addition-Reactions. *J. Chem. Phys.* **1991**, *94*, 2794–2806.

(30) Heming, M.; Roduner, E. Formation and Dynamics of a SiO2-Adsorbed Radical Observed by Muon Spin Rotation. *Surf. Sci.* **1987**, *189*, 535–542. Heming, M. Modern Epr-Related Methods in Surface Science and Heterogeneous Catalysis. *Z. Phys. Chem.* **1987**, *151*, 35–50.

(31) Fleming, D. G.; Shelley, M. Y.; Arseneau, D. J.; Senba, M.; Pan, J. J.; Roduner, E. Hyperfine and host-guest interactions of the Mu-cyclohexadienyl radical in NaY zeolite. *J. Phys. Chem. B* **2002**, *106*, 6395–6407.

(32) McKenzie, I; Addison-Jones, B; Brodovitch, J-C; Ghandi, K; Percival, P. W. Structure and dynamics of the Mu adduct of diketene. *PhysChemComm* **2001**, *27*, 1–3.

(33) Roduner, E.; Stolmar, M.; Dilger, H.; Reid, I. D. Reorientational dynamics of cyclohexadienyl radicals in high-silica ZSM-5. *J. Phys. Chem. A* **1998**, *102*, 7591–7597.

(34) Wu, F.; Chen, X. J.; Shan, X.; Tian, S. X.; Li, Z. J.; Xu, K. Z. Conformational stability of 1-butene: An electron momentum spectroscopy investigation. *J. Phys. Chem. A* **2008**, *112*, 4360–4366.

(35) Improta, R.; Barone, V. Interplay of electronic, environmental, and vibrational effects in determining the hyperfine coupling constants of organic free radicals. *Chem. Rev.* **2004**, *104*, 1231–1253.

(36) Thomas, S. L.; Carmichael, I. Hyperfine interactions in muonium-containing radicals. *Physica B-Condens. Matter* **2006**, *374*, 290–294.

(37) Barone, V. Anharmonic vibrational properties by a fully automated second-order perturbative approach. *J. Chem. Phys.* **2005**, *122*, 014108.

(38) Claxton, T. A.; Graham, A. M.; Cox, S. F. J.; Maric, D. M.; Meier, P. F.; Vogel, S. Vibrationally Averaged Spin-Densities on Muons and Protons in the Hydroxyl and Ethyl Radicals. *Hyperfine Interact.* **1990**, *65*, 913–926.

(39) Johnson, P. M.; Sears, T. J. Vibrational effects on the torsional motion of ethyl radical. *J. Chem. Phys.* **1999**, *111*, 9222–9226.

(40) Carmichael, I. Private communication. Unpublished ab-initio calculations. Dept. of Chemistry and Radiation Chemistry Laboratory, Notre Dame University.

(41) Shiotani, M.; Isamoto, N.; Hayashi, M.; Fänhström, T.; Lunnel, S. Deuterium isotope effects on rotation of methyl hydrogens. A study of the dimethyl ether radical cation by ESR spectroscopy and ab initio and density functional theory. *J. Am. Chem. Soc.* **2000**, *122*, 12281–12288.

(42) Mitov, S.; Panchenko, A.; Roduner, E. Spin polarization, delocalization, and the effect of nonplanarity in hyperfine coupling constants of perfluorinated alkyl radicals. *J. Phys. Chem. A* **2007**, *111*, 5294–5299.

(43) Vujošević, D.; Dilger, H.; McKenzie, I.; Martyniak, A.; Scheuermann, R.; Roduner, E. *J. Phys. Chem. B* **2007**, *111*, 199–208.